confirmed in BDL $SR^{-/-}$ mice, which had reduced levels of phosphorylated ERK1/2 in isolated large cholangiocytes. As expected, large cholangiocytes isolated from $SR^{-/-}$ did not respond to secretin, which was evidenced by lack of accumulation of intracellular cAMP levels.

Finally, we demonstrated that SR expression is critical for basal cholangiocyte proliferation in large mouse cholangiocytes that have stable knockdown of SR by transfection with short hairpin RNA for SR. These SR stable knockdown cells displayed decreased basal and secretin-stimulated proliferative capacity compared with control-transfected cholangiocytes. As expected, these stable knockdown SR cells lacked secretin-stimulated intracellular cAMP levels. Decreased basal proliferative rates that we observed in the cells with stable knockdown of SR compared with the mock-transfected controls are suggestive of the regulation of the basal proliferative rates by secretin perhaps in an autocrine mechanism. Consistent with our current study, we have previously shown that secretin stimulates the proliferation of two normal human cholangiocyte cell lines: H-69 and HiBEpiC.[26] Collectively, the findings of our study revealed that secretin is a trophic factor for cholangiocytes that differentially regulated the growth of large cholangiocytes by acting on the specifically expressed SR under normal and pathological conditions.

De novo SR expression in small cholangiocytes is often found in models of liver damage that alter the SR-dependent functional capacity of large cholangiocytes such as CCl_4 acute hepatoxicity.[14] We also have preliminary findings (unpublished data) that suggest that secretin has a protective role versus CCl_4-induced damage of large cholangiocytes.[14] These findings are consistent with the lack of secretin-dependent signaling resulting in an increase in the basal apoptotic activity in cells lacking SR that we observed in the SR knockdown cells. In addition, our other studies in which large cholangiocyte damage was prevented by administration of bile acids (such as taurocholate)[32] and cAMP agonists[30] suggest that secretin, a cAMP agonist, would have a role as a protective factor during large bile duct damage. Further studies are necessary to confirm this role, but are suggestive that secretin or other cAMP agonists could prevent biliary loss in ductopenia pathologies such as drug-induced vanishing bile duct syndrome or graft versus host disease.

The discovery of a novel proproliferative function of secretin in cholangiocytes, along with the demonstration that *in vitro* and *in vivo* molecular manipulations of the SR gene ablated the proliferative and apoptotic responses of large cholangiocytes, may shed light on the development of new therapeutic approach for the management of cholestatic liver diseases. Overexpression of SR or secretin administration might open new avenues for the treatment of ductopenic liver diseases.

References

1. Alpini G, Glaser S, Robertson W, Rodgers RE, Phinizy JL, Lasater J, et al. Large but not small intrahepatic bile ducts are involved in secretin-regulated ductal bile secretion. Am J Physiol Gastrointest Liver Physiol 1997;272:G1064-G1074.
2. Alpini G, Lenzi R, Sarkozi L, Tavoloni N. Biliary physiology in rats with bile ductular cell hyperplasia. Evidence for a secretory function of proliferated bile ductules. J Clin Invest 1988;81:569-578.
3. Kanno N, LeSage G, Glaser S, Alpini G. Regulation of cholangiocyte bicarbonate secretion. Am J Physiol Gastrointest Liver Physiol 2001; 281:G612-G625.
4. Alpini G, Roberts S, Kuntz SM, Ueno Y, Gubba S, Podila PV, et al. Morphological, molecular, and functional heterogeneity of cholangiocytes from normal rat liver. Gastroenterology 1996;110:1636-1643.
5. Glaser S, Gaudio E, Rao A, Pierce LM, Onori P, Franchitto A, et al. Morphological and functional heterogeneity of the mouse intrahepatic biliary epithelium. Lab Invest 2009;89:456-469.
6. Martinez-Anso E, Castillo JE, Diez J, Medina JF, Prieto J. Immunohistochemical detection of chloride/bicarbonate anion exchangers in human liver. HEPATOLOGY 1994;19:1400-1406.
7. Kato A, Gores GJ, LaRusso NF. Secretin stimulates exocytosis in isolated bile duct epithelial cells by a cyclic AMP-mediated mechanism. J Biol Chem 1992;267:15523-15529.
8. Ueno Y, Alpini G, Yahagi K, Kanno N, Moritoki Y, Fukushima K, et al. Evaluation of differential gene expression by microarray analysis in small and large cholangiocytes isolated from normal mice. Liver Int 2003;23:449-459.
9. Alpini G, Ulrich C, Roberts S, Phillips JO, Ueno Y, Podila PV, et al. Molecular and functional heterogeneity of cholangiocytes from rat liver after bile duct ligation. Am J Physiol Gastrointest Liver Physiol 1997; 272:G289-G297.
10. Banales JM, Arenas F, Rodriguez-Ortigosa CM, Saez E, Uriarte I, Doctor RB, et al. Bicarbonate-rich choleresis induced by secretin in normal rat is taurocholate-dependent and involves AE2 anion exchanger. HEPATOLOGY 2006;43:266-275.
11. Lazaridis KN, Strazzabosco M, LaRusso NF. The cholangiopathies: disorders of biliary epithelia. Gastroenterology 2004;127:1565-1577.
12. Alpini G, Glaser S, Ueno Y, Pham L, Podila PV, Caligiuri A, et al. Heterogeneity of the proliferative capacity of rat cholangiocytes after bile duct ligation. Am J Physiol Gastrointest Liver Physiol 1998;274: G767-G775.
13. LeSage G, Glaser S, Gubba S, Robertson WE, Phinizy JL, Lasater J, et al. Regrowth of the rat biliary tree after 70% partial hepatectomy is coupled to increased secretin-induced ductal secretion. Gastroenterology 1996;111:1633-1644.
14. LeSage G, Glaser S, Marucci L, Benedetti A, Phinizy JL, Rodgers R, et al. Acute carbon tetrachloride feeding induces damage of large but not small cholangiocytes from BDL rat liver. Am J Physiol Gastrointest Liver Physiol 1999;276:G1289-G1301.
15. Alvaro D, Onori P, Metalli VD, Svegliati-Baroni G, Folli F, Franchitto A, et al. Intracellular pathways mediating estrogen-induced cholangiocyte proliferation in the rat. HEPATOLOGY 2002;36:297-304.
16. Alpini G, Lenzi R, Zhai WR, Slott PA, Liu MH, Sarkozi L, et al. Bile secretory function of intrahepatic biliary epithelium in the rat. Am J Physiol Gastrointest Liver Physiol 1989;257:G124-G133.
17. Alpini G, Ulrich CD 2nd, Phillips JO, Pham LD, Miller LJ, LaRusso NF. Upregulation of secretin receptor gene expression in rat

cholangiocytes after bile duct ligation. Am J Physiol Gastrointest Liver Physiol 1994;266:G922-G928.
18. Glaser S, Benedetti A, Marucci L, Alvaro D, Baiocchi L, Kanno N, et al. Gastrin inhibits cholangiocyte growth in bile duct-ligated rats by interaction with cholecystokinin-B/Gastrin receptors via D-myo-inositol 1,4,5-triphosphate-, $Ca^{(2+)}$-, and protein kinase C alpha-dependent mechanisms. HEPATOLOGY 2000;32:17-25.
19. Lam IP, Siu FK, Chu JY, Chow BK. Multiple actions of secretin in the human body. Int Rev Cytol 2008;265:159-190.
20. Glaser S, Ueno Y, DeMorrow S, Chiasson VL, Katki KA, Venter J, et al. Knockout of alpha-calcitonin gene-related peptide reduces cholangiocyte proliferation in bile duct ligated mice. Lab Invest 2007;87: 914-926.
21. Chu JY, Chung SC, Lam AK, Tam S, Chung SK, Chow BK. Phenotypes developed in secretin receptor-null mice indicated a role for secretin in regulating renal water reabsorption. Mol Cell Biol 2007;27: 2499-2511.
22. Miyoshi H, Rust C, Roberts PJ, Burgart LJ, Gores GJ. Hepatocyte apoptosis after bile duct ligation in the mouse involves Fas. Gastroenterology 1999;117:669-677.
23. DeMorrow S, Francis H, Gaudio E, Ueno Y, Venter J, Onori P, et al. Anandamide inhibits cholangiocyte hyperplastic proliferation via activation of thioredoxin 1/redox factor 1 and AP-1 activation. Am J Physiol Gastrointest Liver Physiol 2008;294:G506-G519.
24. Strausberg RL, Feingold EA, Grouse LH, Derge JG, Klausner RD, Collins FS, et al. Generation and initial analysis of more than 15,000 full-length human and mouse cDNA sequences. Proc Natl Acad Sci USA 2002;99:16899-16903.
25. Baumgardner JN, Shankar K, Hennings L, Badger TM, Ronis MJ. A new model for nonalcoholic steatohepatitis in the rat utilizing total enteral nutrition to overfeed a high-polyunsaturated fat diet. Am J Physiol Gastrointest Liver Physiol 2008;294:G27-G38.
26. Onori P, Wise C, Gaudio E, Franchitto A, Francis H, Carpino G, et al. Secretin inhibits cholangiocarcinoma growth via dysregulation of the cAMP-dependent signaling mechanisms of secretin receptor. Int J Cancer 2009; doi:10.1002/ijc.25028.
27. Korner M, Hayes GM, Rehmann R, Zimmermann A, Scholz A, Wiedenmann B, et al. Secretin receptors in the human liver: expression in biliary tract and cholangiocarcinoma, but not in hepatocytes or hepatocellular carcinoma. J Hepatol 2006;45:825-835.
28. Alvaro D, Mancino MG, Glaser S, Gaudio E, Marzioni M, Francis H, et al. Proliferating cholangiocytes: a neuroendocrine compartment in the diseased liver. Gastroenterology 2007;132:415-431.
29. Francis H, Glaser S, Ueno Y, LeSage G, Marucci L, Benedetti A, et al. cAMP stimulates the secretory and proliferative capacity of the rat intrahepatic biliary epithelium through changes in the PKA/Src/MEK/ERK1/2 pathway. J Hepatol 2004;41:528-537.
30. LeSage G, Alvaro D, Benedetti A, Glaser S, Marucci L, Baiocchi L, et al. Cholinergic system modulates growth, apoptosis, and secretion of cholangiocytes from bile duct-ligated rats. Gastroenterology 1999;117: 191-199.
31. Banales JM, Masyuk TV, Gradilone SA, Masyuk AI, Medina JF, LaRusso NF. The cAMP effectors Epac and protein kinase a (PKA) are involved in the hepatic cystogenesis of an animal model of autosomal recessive polycystic kidney disease (ARPKD). HEPATOLOGY 2009;49: 160-174.
32. Marzioni M, LeSage GD, Glaser S, Patel T, Marienfeld C, Ueno Y, et al. Taurocholate prevents the loss of intrahepatic bile ducts due to vagotomy in bile duct-ligated rats. Am J Physiol Gastrointest Liver Physiol 2003;284:G837-G852.

Research Article

EASL EUROPEAN ASSOCIATION FOR THE STUDY OF THE LIVER | JOURNAL OF HEPATOLOGY

Possible involvement and the mechanisms of excess *trans*-fatty acid consumption in severe NAFLD in mice

Noriyuki Obara[1], Koji Fukushima[1], Yoshiyuki Ueno[1,*], Yuta Wakui[1], Osamu Kimura[1], Keiichi Tamai[1], Eiji Kakazu[1], Jun Inoue[1], Yasuteru Kondo[1], Norihiko Ogawa[2], Kenta Sato[3], Tsuyoshi Tsuduki[3], Kazuyuki Ishida[4], Tooru Shimosegawa[1]

[1]*Division of Gastroenterology, Tohoku University Graduate School of Medicine, 1-1 Seiryo, Aobaku, Sendai 980-8574, Japan;* [2]*Division of Advanced Surgical Science and Technology, Graduate School of Medicine, Tohoku University, Sendai, Japan;* [3]*Laboratory of Food and Biomolecular Science, Graduate School of Agricultural Science, Tohoku University, Sendai, Japan;* [4]*Department of Pathology, Tohoku University Hospital, Sendai, Japan*

Background & Aims: Excessive *trans*-fatty acids (TFA) consumption has been thought to be a risk factor mainly for coronary artery diseases while less attention has been paid to liver disease. We aimed to clarify the impact of TFA-rich oil consumption on the hepatic pathophysiology compared to natural oil.

Methods: Mice were fed either a low-fat (LF) or high-fat (HF) diet made of either natural oil as control (LF-C or HF-C) or partially hydrogenated oil, TFA-rich oil (LF-T or HF-T) for 24 weeks. We evaluated the liver and body weight, serological features, liver lipid content and composition, liver histology and hepatic lipid metabolism-related gene expression profile. In addition, primary cultures of mice Kupffer cells (KCs) were evaluated for cytokine secretion and phagocytotic ability after incubation in *cis*- or *trans*-fatty acid-containing medium.

Results: The HF-T-fed mice showed significant increases of the liver and body weights, plasma alanine-aminotransferase, free fatty acid and hepatic triglyceride content compared to the HF-C group, whereas the LF-T group did not differ from the LF-C group. HF-T-fed mice developed severe steatosis, along with increased lipogenic gene expression and hepatic TFA accumulation. KCs showed increased tumor necrosis factor secretion and attenuated phagocytotic ability in the TFA-containing medium compared to its *cis*-isomer.

Conclusions: Excessive consumption of the TFA-rich oil up-regulated the lipogenic gene expression along with marked hepatic lipid accumulation. TFA might be pathogenic through causing severe steatosis and modulating the function of KCs. The quantity and composition of dietary lipids could be responsible for the pathogenesis of non-alcoholic steatohepatitis.

Keywords: *trans*-Fatty acid; NASH; NAFLD; Metabolic syndrome; Kupffer cell.
Received 16 September 2009; received in revised form 18 January 2010; accepted 26 February 2010; available online 22 April 2010
*Corresponding author. Tel.: +81 22 717 7171; fax: +81 22 717 7177.
E-mail address: yueno@mail.tains.tohoku.ac.jp (Y. Ueno).

Abbreviations: NAFLD, non-alcoholic fatty liver disease; NASH, non-alcoholic steatohepatitis; FFA, free fatty acid; LPS, lipopolysaccharide; TFA, *trans*-fatty acid; ALT, alanine-aminotransferase; LF(-C or -T), low-fat (control or TFA-rich) diet; HF(-C or -T), high-fat (control or TFA-rich) diet; KCs, Kupffer cells (KCs); AST, aspartate-aminotransferase; TG, triglyceride; ELISA, Enzyme-Linked ImmunoSorbent Assay; HDL, high density lipoprotein; (V)LDL, (very) low density lipoprotein; NAS, NAFLD activity score; TBARS, thiobarbituric acid reactive substances; TNFα, tumor necrosis factor α; IL-6, interleukin-6; SD, standard deviation; iNOS, inducible nitric oxide synthase; TGF-β, transforming growth factor-β; SREBP-1, sterol regulatory element-binding protein-1; FAS, fatty acid synthase; ACC, acetyl CoA carboxylase; PPAR, peroxisome proliferator activated receptor; PGC-1β, PPARγ coactivator-1β; PUFA, polyunsaturated fatty acid; MUFA, monounsaturated fatty acid; SFA, saturated fatty acid.

Introduction

In concordance with the prevalence of obesity, the incidence of non-alcoholic fatty liver disease (NAFLD) has increased and is nowadays recognized as the most common liver disease [2]. It is known that a part of NAFLD can progress to non-alcoholic steatohepatitis (NASH), liver fibrosis, cirrhosis and hepatocellular carcinoma [9]. Nevertheless, the mechanisms of NAFLD-to-NASH transition remain to be clarified; NAFLD appears to originate from the dysregulation of hepatic lipid metabolism as a part of the metabolic syndrome accompanied by visceral obesity, dyslipidemia, atherosclerosis, and insulin resistance [25]. According to the hypothetical theory named the 2-hit theory [5], the secondary hit to NAFLD that can be due to free fatty acid (FFA)s, oxidative stress, lipopolysaccharide (LPS) and inflammatory cytokines, causes NASH as a consequence.

In terms of the "first hit", the lipid accumulation in the liver is induced by high-fat diets [6,23] that include various lipid species. Such dietary lipid species uniquely affect the obesity phenotype, liver histology and gene expression pattern in the rat liver [3]. In this context, lipid species could play a potential role in the pathogenesis of NAFLD and/or NASH.

trans-Fatty acid (TFA) is produced through the industrial hardening of the vegetable oils to make the products more stable and robust, and thus easier to handle or store. Excess consumption of TFA is known as a risk factor for coronary artery diseases, insulin resistance and obesity accompanied by systemic inflammation, the features of metabolic syndrome [20,29]. Nevertheless, little is known about the effects on the liver induced by lipids.

ELSEVIER

Journal of Hepatology **2010** vol. 53 | 326–334

Fast-foods, containing large amount of TFA in the form of margarine, spreads or frying oils, cause body-weight gain and abnormal serum alanine-aminotransferase (ALT) elevations in healthy subjects [15]. In addition, TFA-rich chow leads to hepatic steatosis [30], ALT elevations and insulin resistance in mice [17]; although the mechanisms have not been completely clarified. Therefore, we aimed to investigate the impact of the dietary lipid species and their quantities on the pathogenicity of hepatic inflammation and steatosis in mice comparing in particular natural oil and industrially produced partially hydrogenated TFA-rich oil of the same origin.

Materials and methods

Animal treatment

All the animal experiments were conducted under the approval of the Institutional Animal Care and Use Committees of Tohoku University. Female C57BL/6Njcl mice (8–10 weeks) were randomly assigned to four groups ($n = 6$ per group) and fed the designated chows (ORIENTAL YEAST Co. Ltd., Tokyo, Japan) *ad libitum* for 24 weeks, respectively. Low-fat diet (LF) and high-fat diet (HF) were made of either natural canola oil as control oil (LF-C and HF-C) or industry produced partially hydrogenated canola oil as TFA-rich oil (28.5% TFA/total fat, LF-T and HF-T), respectively (Table 1). After 12 h of fasting, the mice were sacrificed under diethylether anesthesia and the livers were removed and weighed. The divided livers were either stored at −80 °C for lipid, protein and gene expression analysis, or fixed in 4% paraformaldehyde and embedded in paraffin for histological evaluation. Standard chow-fed female C57BL/6Njcl mice (6–10 weeks) were used as a source of primary Kupffer cells (KCs).

Chemistry

Plasma aspartate-aminotransferase (AST), ALT, triglyceride (TG) and total cholesterol were measured with FUJI DRI-CHEM 7000 (FUJIFILM, Tokyo, Japan) at Biomedical Research Core of Tohoku University Graduate School of Medicine. Plasma adiponectin (AdipoGen, Seoul, Korea) and leptin (RayBio, GA, USA) were measured by Enzyme-Linked ImmunoSorbent Assay (ELISA). Plasma FFA, high density lipoprotein (HDL)-cholesterol and (very) low density lipoprotein ((V)LDL)-cholesterol were measured by enzymatic assay kits (BioVision, CA, USA).

Histology and immunohistochemistry

The thin-sliced specimens were stained with hematoxylin and eosin to evaluate steatosis and inflammation or Sirius red to evaluate fibrosis of the liver. The histology was scored by the NAFLD activity score (NAS) [16]. KCs were stained with anti-F4/80 monoclonal antibody (Abcam, Cambridge, UK) and neutrophils were detected by myeroperoxidase immunostaining (Abcam). Apoptosis was evaluated by TUNEL method using an ApopTag kit (Chemicon, CA, USA).

Table 1. Diet compositions.

	Low-fat diet		High-fat diet	
	Control oil (LF-C) kcal%	TEA-rich oil (LF-T) kcal%	Control (HF-C) kcal%	TEA-rich (HF-T) kcal%
Diet compositions				
Protein	13.8	13.8	18.8	18.8
Carbohydrate	74.4	74.4	17.6	17.6
Over all fat	11.8	11.8	63.6	63.6
Fat composition (g/100 g)				
Saturated	7.8	21.7	7.8	21.7
(*cis*-)Monounsaturated	62.5	45.3	62.5	45.3
Polyunsaturated	29.7	4.5	29.7	4.5
trans- (%)		28.5		28.5

Immunoblot analysis and real-time RT-PCR

Liver protein extracts were evaluated by immunoblot analysis with the following primary antibodies: phosphor-AKT (Thr308 and Ser473), total AKT (Cell Signaling Technology, Danvers, MA) and β-actin (Sigma, MO, USA). RNA extracted from the livers was subjected to real-time RT-PCR analysis using the specifically designed primer sets purchased form TAKARA BIO Perfect Real Time Support System (TAKARA BIO INC., Tokyo, Japan) and One Step SYBR Prime Script RT-PCR Kit II (TAKARA BIO INC.), and only PGC-1β was analyzed using the specifically designed TaqMan primer set and 1-step kit (Applied Biosystems, CA, USA). All results were normalized by GAPDH as the internal control.

Lipidomic analysis of the liver

Hepatic TG and FFA content were measured by enzymatic assay kit (BioVision) and were normalized by the liver weight. Hepatic lipid peroxide was evaluated by measuring TBARS (thiobarbituric acid reactive substances, Cayman Chemical Company, USA) in the liver and was normalized by the protein level [18]. Total lipids from the liver were extracted by Folch's procedure [10]. The lipids were methylated and evaluated by gas chromatography as previously reported [31].

Isolation and culture of primary Kupffer cells

KCs were isolated as reported previously [28]. Briefly, the mice livers were digested by two-step collagenase perfusion. The minced livers were subjected to the gradient centrifugation of Percoll (Sigma) and succeeding counterflow centrifugal elutriation. The viabilities of the obtained cells evaluated by trypan blue staining were more than 85%, and the purity was more than 90% determined by the population of CD11b positive cells counted by FACS Calibur (Becton Dickinson, Tokyo, Japan). KCs were suspended in RPMI1640 medium with 10% fetal bovine serum and antibiotics (100 U/ml penicillin G, 100 μg/ml streptomycin sulfate) and incubated overnight at 37 °C in 5% CO_2 incubator for the succeeding examinations.

Fatty acid treatment

Fatty acids (Larodan Fine Chemicals, Malmo, Sweden) were dissolved in RPMI1640 medium with 1% fatty acid-free bovine serum albumin (Calbiochem, Darmstadt, Germany) and adjusted to a final concentration of 200 μM with 1% bovine serum albumin, 1% ITS-A supplement (GIBCO, CA, USA) and antibiotics same as above. After overnight incubation, KCs were washed and the medium was changed to fatty acid-containing medium or fatty acid-free medium as the control, and incubated for another 24 h.

Cytokine production by KCs stimulated with lipopolysaccharide

After 24 h incubation, KCs were stimulated by LPS (100 ng/ml, SIGMA) combined with LPS-binding protein (200 pg/ml, ALEXIS BIOCHEMICALS, Lausanne, Switzerland) for 6 h, and the cell viability was determined by MTS assay (3-(4,5-dimethylthiazol-2-yl)-5-(3-carboxymethoxyphenyl)-2-(4-sulfophenyl)-2*H*-tetrazolium, inner salt and phenazine ethosulfate, Promega, Tokyo, Japan). The supernatants were subjected to ELISA (Thermo Fisher Scientific Inc., IL, USA) for the evaluation of the tumor necrosis factor-alfa (TNFα) and interleukin-6 (IL-6) production.

Phagocytotic ability of KCs

After 24 h incubation, KCs were incubated at 37 °C for 1 h with 1 μm latex beads (75 ng/ml, SIGMA) or at 4 °C in the fatty acid-free medium as control. After incubation, the cells were washed 3 times, detached with trypsin/EDTA and analyzed by FACS calibur [1].

Statistical analysis

The results are shown as the mean ± standard deviation (SD), and were analyzed by SPSS software (SPSS INC., Tokyo, Japan).

The differences between the groups were tested by ANOVA, followed by Tukey post hoc test. A p values less than 0.05 were considered statistically significant.

Results

Physiological and biochemical characteristics

Body weight was similar between LF-fed mice, increased in HF-fed mice compared to LF-fed mice, and strikingly HF-T-fed mice weighed 1.3-fold more than HF-C-fed mice (Table 2). Liver weight was significantly increased in only HF-T-fed mice by approximately 2-fold compared to the other groups. The liver–body weight ratio was significantly increased by 1.2- and 1.6-fold in LF-T-fed and HF-T-fed mice, respectively, compared to the corresponding control groups with the same dietary composition, and decreased by approximately 20% in the HF-C-fed mice compared to the LF-C-fed mice.

Plasma AST, ALT, TG, FFA and leptin were similar between the LF groups irrespective of the dietary lipid source, but in the LF-T group, total cholesterol, HDL-cholesterol, (V)LDL-cholesterol and adiponectin were significantly decreased compared to the LF-C group (Table 2). In contrast, some serum markers were elevated in the HF-T group compared to the HF-C group, particularly AST, ALT, TG, total cholesterol, (V)LDL-cholesterol, FFA and leptin were significantly increased. As for the control oil-fed mice, total cholesterol, HDL-cholesterol, (V)LDL-cholesterol and adiponectin were lower, whereas plasma leptin was higher in HF-C-fed than in LF-C-fed mice. Between TFA-rich oil-fed mice, all serum markers except adiponectin were also significantly higher in HF-T-fed than in LF-T-fed mice.

Liver histology

There were few lipid droplets in LF-C-fed mice liver. Mild microvesicular and macrovesicular steatosis was present around zone 1 in LF-T-fed mice livers and abundant large lipid droplets around zones 1 and 2 in HF-C-fed mice livers. Inflammation and ballooning degeneration were minimal in these groups (Fig. 1A). However, the HF-T-fed mice livers were characterized by foamy, prominent microvesicular steatosis throughout the lobe and some macrovesicular lipid droplets in zones 1 and 2. Most of the hepatocytes were expanded with marked small lipid droplets that surrounded the nuclei, and the severely expanded hepatocytes presented the phenotype of ballooning degeneration (Fig. 1A); moreover, some of the fatty hepatocytes were surrounded by infiltrated neutrophils confirmed by immunostaining for myeloperoxidase, forming lipogranuloma (Fig. 1B) accompanied by ballooning hepatocytes (Fig. 1C). The number of neutrophils was increased in HF-T-fed mice livers (Fig. 1D). However, when evaluated by NAS, the HF-T group did not show significant differences (Table 2).

To investigate the involvement of KCs in the pathological difference between the HF-C group and HF-T group, we performed immunohistochemical staining for F4/80, a macrophage-restricted surface glycoprotein. F4/80-positive cells were more prevalent in the HF-T group (Fig. 1E). Although fibrosis was not identified visually by Sirius red staining in any of the groups (not shown), collagen type1, α1 mRNA expression in the liver, as an early fibrosis marker, increased only in HF-T-fed mice by 3.6-fold compared to LF-C-fed mice (Fig. 1F). TUNEL assay did not reveal conspicuous apoptotic hepatocytes in each group, however some non-parenchymal cells were TUNEL positive (Supplementary Fig. 1).

Lipid and lipid peroxide content and fatty acid composition of liver

The hepatic total lipid (Fig. 2A), TG (Fig. 2B), FFA (Fig. 2C) and lipid peroxide contents (Fig. 2D) did not differ between the LF-C and LF-T groups. On the other hand, reflecting the marked liver weight gain and histological steatotic changes, hepatic total lipid, TG and lipid peroxide content were significantly increased in the HF-T group compared to the HF-C group, while FFA content did not differ. All of these markers had a tendency to be elevated in the HF groups compared to the LF groups and when compared between the corresponding dietary oil-fed groups, although the TG increase in HF-C-fed mice was not statistically significant.

Table 2. Influence of *trans*-fatty acid-rich oil intake for the physiological and biochemical characteristics.

	Low-fat diet		High-fat diet	
	Control oil (LF-C)	TFA-rich oil (LF-T)	Control oil (HF-C)	TFA-rich oil (HF-T)
Body weight (g)	24.4 ± 2.1	23.1 ± 1.3	31.8 ± 3.6‡	40.9 ± 7.0*‡†
Liver weight (g)	1.08 ± 0.16	1.22 ± 0.08	1.11 ± 0.11	2.40 ± 1.01*‡†
Liver–body weight ratio (%)	4.5 ± 0.4	5.4 ± 0.2*	3.5 ± 0.3‡	5.6 ± 1.6*†
Plasma characteristics				
Aspartate-aminotransferase (IU/L)	95.2 ± 12.4	82.5 ± 20.8	136.8 ± 47.0	262.2 ± 72.0*‡†
Alanine-aminotransferase (IU/L)	48.8 ± 15.0	37.0 ± 7.3	50.4 ± 10.9	244.0 ± 105.7*‡†
Triglyceride (mg/dl)	60.3 ± 19.2	51.0 ± 12.8	62.4 ± 14.8	124.8 ± 45.0*‡†
Total cholesterol (mg/dl)	77.0 ± 8.9	47.5 ± 6.1*	55.2 ± 5.0	87.8 ± 10.1*‡
HDL-cholesterol (mg/dl)	51.6 ± 8.3	26.2 ± 3.9*	33.3 ± 7.2‡	38.6 ± 5.0‡†
(V)LDL-cholesterol (mg/dl)	16.8 ± 2.1	12.0 ± 1.5*	11.9 ± 1.0‡	17.4 ± 1.7*‡
Free fatty acids (nmol/ml)	1.77 ± 0.38	1.43 ± 0.31	1.99 ± 0.58	3.64 ± 0.42*‡†
Adiponectin (μg/ml)	25.5 ± 1.4	18.2 ± 1.4*	20.0 ± 1.5‡	20.0 ± 1.4†
Leptin (ng/L)	5.6 ± 0.7	5.3 ± 0.6	13.8 ± 2.0‡	23.7 ± 2.3*††
Total: HDL-cholesterol ratio	1.54 ± 0.06	2.33 ± 0.5*	1.71 ± 0.37	2.25 ± 0.87†
NAFLD activity score				
Steatosis	0.33 ± 0.52	0.17 ± 0.41	1.67 ± 0.82‡	1.17 ± 0.41‡
Inflammation	0.33 ± 0.52	0.33 ± 0.52	0.83 ± 0.75	1.00 ± 0.63
Ballooning	0.00 ± 0.00	1.00 ± 0.63*	1.00 ± 0.00‡	1.67 ± 0.82†

All values are means ± SD (n = 6 per each group).

* Significantly different from the corresponding control group with the same dietary composition; p <0.05.

‡ Significantly different from the low-fat diet with the same dietary lipid as a source; p <0.05.

† Significantly different from low-fat control diet group; p <0.05.

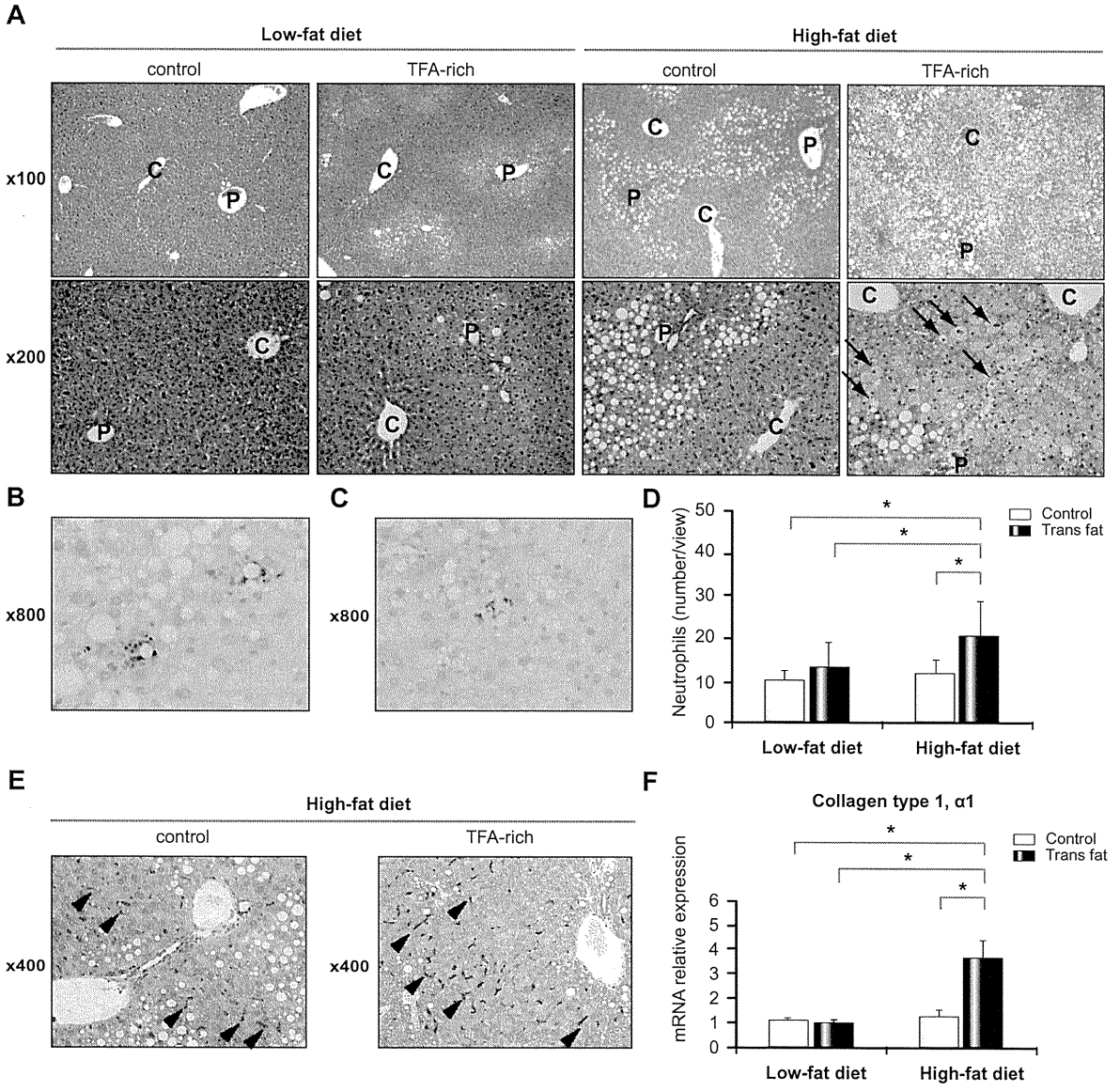

Fig. 1. Distinct steatotic features of the liver. (A) Representative liver histology stained with H&E. Remarkably expanded hepatocytes with extensive small lipid droplets make a feature of ballooning degeneration (arrows). Neutrophils confirmed by myeloperoxidase staining were (B) forming lipogranulomas and (C) surrounding the ballooning degenerated hepatocytes. (D) The number of neutrophils is increased in HF-T-fed mice liver. (E) KCs were detected by anti-F4/80 immunohistochemical staining (arrow heads). (F) Quantitative RT-PCR revealed elevation of collagen type 1, α1 mRNA expression in liver of HF-T-fed mice. P, portal tract; C, central vein. *p <0.05.

We evaluated the lipid composition of the liver to examine the pathological condition in the model. Compared to the LF-C group, the sum of total polyunsaturated fatty acid (PUFA), n-6 PUFA and n-3 PUFA was decreased in the LF-T group, but did not differ significantly in the other groups (Fig. 2E.). In the HF-C group, the sum of saturated fatty acid (SFA) and monounsaturated fatty acid (MUFA) was decreased, and total PUFA, n-6 PUFA and n-3 PUFA were increased compared to the LF-C group. However, in the HF-T group, total PUFA and n-6 PUFA decreased significantly compared to the LF-C group, and their proportions were similar to those of the LF-T group. The potentially beneficial lipid n-3 PUFA that is thought to prevent insulin resistance and hepatic steatosis [11], was increased even in the HF-T group compared to the LF-T group, the level of which was similar to that of the LF-C group.

The content of individual fatty acids in the liver coordinated nearly synergistically with the sum of the content of the fatty acids in the same unsaturation grade (Fig. 2E and Table 3). The unique accumulation of elaidic acid (18:1(9-*trans*)), chief component of dietary TFA, was noteworthy in the LF-T and HF-T groups. The content of arachidonic acid (20:4n-6) alone decreased to 70% only in the HF-T group, which was similar to the LF-T group in

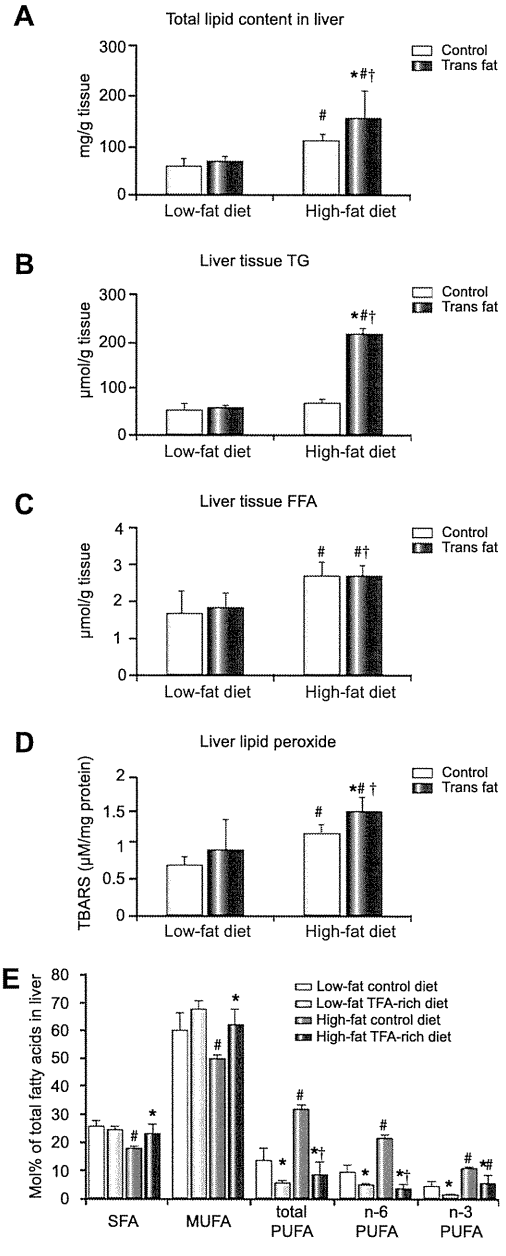

Fig. 2. Lipid accumulation in the liver. (A) Total lipid, (B) TG, and (C) FFA in the liver were measured and normalized to the tissue weight. (D) Lipid peroxide in the liver was measured and normalized by each amount of protein. (E) The hepatic fatty acid composition analyzed by gas chromatography was organized as follows: SFA, saturated fatty acid; MUFA, *cis*-monounsaturated fatty acid; PUFA, polyunsaturated fatty acid; *n*-6, *n*-6 PUFA; and *n*-3, *n*-3 PUFA ($n = 6$ for each group). *Significantly different from the control group with the same dietary composition; ‡significantly different from the low-fat diet with same dietary oil; †significantly different from LF-C-fed and HF-T-fed group.

terms of linoleic acid (18:2*n*-6), the precursor of arachidonic acid. Except for elaidic acid and arachidonic acid, there were no specific alterations for the HF-T group.

Cytokine-, adipokine- and lipid metabolism-related gene expression in liver

Real-time RCR showed that TNFα and inducible nitric oxide synthase (iNOS) mRNA expression increased in the HF groups compared to the LF groups by approximately 2-fold when evaluated for each C or T group (Table 4), while no difference was seen in IL-6 and transforming growth factor-β (TGF-β) mRNA expression in liver among all groups. In addition, adiponectin receptor 1 and 2 gene expression was measured as adipokine related genes, but they did not differ among all groups.

To examine the potential mechanisms of hepatic steatosis by the TFA-rich diet, we determined the expression of known mediators of lipogenesis, fatty acid oxidation and TG excretion in liver, the imbalance of which is thought to lead to steatosis. Sterol regulatory element-binding protein-1 (SREBP-1) induces fatty acid synthase (FAS) and acetyl CoA carboxylase (ACC), and is implicated in steatosis [27]. In relation to hepatic fatty acid synthesis, the mRNA expression of SREBP-1 was significantly elevated in the LF-T, HF-C and HF-T groups when compared to the LF-C group, whereas FAS and ACC were elevated significantly only in the HF-T group (Table 4). Peroxisome proliferator activated receptor γ (PPARγ) is also implicated in steatosis [33]. The expression of PPARγ1 did not differ among the groups, while PPARγ2 was significantly elevated 13-fold in the HF-C group and, remarkably, 50-fold in the HF-T group. Although, the expression of PPARγ coactivator-1β (PGC-1β), known to coactivate the SREBP-1 and stimulate lipogenic gene expression [19], was decreased in HF-fed mouse livers. The fatty acid oxidation-related genes of PPARα and carnitine palmitoyl transferase-1, and the TG excretion-related genes of microsomal triglyceride transfer protein and apolipoprotein B did not differ among the groups; fatty acid oxidation-related genes showed a tendency to be decreased in the LF-T group, but without statistical significance.

Concerning cholesterol metabolism-related gene expression in liver, SREBP-2 was increased in the HF groups, but was not affected by the dietary lipid sources. Hydroxymethylglutaryl-CoA synthase-1 and reductase were significantly increased and apolipoprotein A-1, a component of HDL, was decreased only in the HF-T group, while they did not change in the LF-T group, which showed an alteration of plasma cholesterol fraction (Table 4).

Phosphorylation status of AKT in high-fat diet-fed mice livers

As Koppe et al. suggested that TFA feeding increased insulin resistance in mice [17], and to determine if the exacerbating effects of TFA intake on liver were associated with increased insulin resistance, we evaluated the hepatic phosphorylation status of AKT (Fig. 3A). The phospho-AKT(Thr308) level was significantly decreased (Fig. 3B) and the phospho-AKT(Ser473) level was also decreased, but without statistical significance (Fig. 3C) as determined by densitometrical analysis.

TFA increases TNFα production and alters phagocytotic ability of KCs

The *cis*- or *trans*-fatty acid-containing medium showed no cytotoxicity towards KCs when compared to the fatty acid-free control medium (Fig. 4A). TNFα production of KCs induced by LPS was increased in both the C18:1 and C18:2 TFA-containing medium compared to that of *cis*-structural isomer-containing

Table 3. Individual fatty acid composition of the liver.

		Low-fat diet		High-fat diet	
		Control oil (LF-C)	TFA-rich oil (LF-T)	Control oil (HF-C)	TFA-rich oil (HF-T)
SFA					
Myristic	14:0	0.6 ± 0.1	0.5 ± 0.0	0.3 ± 0.1‡	0.4 ± 0.1*†
Palmitic	16:0	21.0 ± 1.6	19.2 ± 1.1	12.1 ± 0.6 ‡	18.7 ± 3.6*
Stearic	18:0	3.7 ± 0.8	3.6 ± 0.6	4.6 ± 0.6	3.3 ± 1.2
Arachidic	20:0	0.6 ± 0.3	1.0 ± 0.1*	0.6 ± 0.3	0.9 ± 0.3
MUFA					
Palmitoleic	16:1 *n*-7	6.9 ± 4.9	7.9 ± 4.8	2.5 ± 0.2	4.9 ± 1.0
Oleic	18:1	53.4 ± 6.7	59.8 ± 2.3	47.4 ± 1.3	57.2 ± 4.8*‡†
Elaidic	18:1 (9-*trans*)	0.0 ± 0.0	2.2 ± 0.5*	0.3 ± 0.2	6.2 ± 2.4*‡†
PUFA					
Linoleic	18:2 *n*-6	6.5 ± 2.1	2.1 ± 0.4*	18.1 ± 1.6‡	2.6 ± 1.4*†
α-Linolenic	18:3 *n*-3	0.6 ± 0.4	0.0 ± 0.0*	3.2 ± 0.5‡	0.2 ± 0.2*
Dihomo-γ-linolenic	20:3 *n*-6	0.2 ± 0.1	0.2 ± 0.1	0.5 ± 0.2‡	0.2 ± 0.2
Arachidonic	20:4 *n*-6	2.5 ± 0.9	2.2 ± 0.5	2.6 ± 0.6	0.6 ± 0.3*‡†
Eicosapentaenoic	20:5 *n*-3	0.4 ± 0.2	0.1 ± 0.0	1.4 ± 0.1‡	1.2 ± 0.9‡†
Docosapentaenoic	22:5 *n*-3	0.2 ± 0.1	0.0 ± 0.0	0.8 ± 0.0‡	0.4 ± 0.3*‡†
Docosahexaenoic	22:6 *n*-3	3.0 ± 1.1	1.0 ± 0.3	5.2 ± 0.4	3.2 ± 2.4

The relative percentage (mean ± SD) of each fatty acid to the total fatty acids is presented ($n = 6$ per each group).
* Significantly different from the corresponding control group with the same dietary composition; $p < 0.05$.
‡ Significantly different from the low-fat diet with the same dietary lipid as a source; $p < 0.05$.
† Significantly different from low-fat control diet group; $p < 0.05$.

medium (Fig. 4B). However, IL-6 production by KCs did not differ between *cis*- and *trans*-fatty acid-containing medium for both C18:1 and C18:2, respectively (Fig. 4C). The phagocytotic ability of KCs incubated in *trans*-C18:1-containing medium was lower than that in *cis*-C18:1-containing medium (Fig. 4D), while the influence of the structural difference of C18:2 fatty acid was small (Fig. 4E).

Discussion

Both of the dietary lipid species [3] and their amounts [6,23] are known to affect hepatic steatosis and inflammation. TFAs have been mainly linked with coronary heart disease, possibly by decreasing HDL-cholesterol and increasing LDL-cholesterol [20,29]; while little attention has been paid to liver disease, even

Table 4. Cytokine-, adipokine- and lipid metabolism-related gene expression in liver.

		Low-fat TFA-rich (LF-T)	High-fat control (HF-C)	High-fat TFA-rich (HF-T)
Cytokine and adipokine				
Tumor necrosis factor	TNF	0.98 ± 0.20	2.11 ± 0.73‡	1.94 ± 0.77‡†
Interleukin-6	IL-6	1.30 ± 0.28	1.16 ± 0.14	1.10 ± 0.25
Transforming growth factor-β	TGB-β	0.86 ± 0.17	1.35 ± 0.50	0.98 ± 0.22
Nitric oxide synthase 2, inducible	iNOS	1.29 ± 0.34	2.23 ± 0.75‡	2.69 ± 0.74‡†
Adiponectin receptor 1	AdipoR1	1.01 ± 0.17	1.29 ± 0.29	1.21 ± 0.25
Adiponectin receptor 2	AdipoR2	0.92 ± 0.16	1.20 ± 0.22	1.28 ± 0.26
Lipogenesis				
Fatty acid synthase	FAS	1.36 ± 0.21	0.79 ± 0.12	1.69 ± 0.46*†
Acetyl-CoA carboxylase	ACC	1.27 ± 0.10	0.80 ± 0.05	1.49 ± 0.37*†
Sterol regulatory element-binding protein-1	SREBP-1	3.76 ± 0.51*	1.93 ± 0.23‡	4.69 ± 0.17*‡†
Peroxisome proliferator activated receptor γ1	PPARγ1	1.45 ± 0.42	1.58 ± 0.48	1.29 ± 0.26
Peroxisome proliferator activated receptor γ2	PPARγ2	1.88 ± 0.33	12.92 ± 6.04‡	50.18 ± 3.61*‡†
PPARγ coactivator-1β	PGC-1β	0.81 ± 0.10	0.61 ± 0.15‡	0.59 ± 0.12‡†
Fatty acid oxidation				
Peroxisome proliferator activated receptor α	PPARα	0.51 ± 0.23	1.25 ± 0.48	1.28 ± 0.41
Carnitine palmitoyl transferase-1	CPT-1	0.63 ± 0.11	1.03 ± 0.34	1.08 ± 0.57
Triglyceride excretion				
Microsomal triglyceride transfer protein	MTP	1.04 ± 0.16	0.92 ± 0.11	0.91 ± 0.11
Apolipoprotein B	ApoB	1.11 ± 0.15	1.20 ± 0.13	1.15 ± 0.09
Cholesterol metabolism				
Sterol regulatory element-binding protein-2	SREBP-2	0.87 ± 0.15	1.66 ± 0.25	1.69 ± 0.34
Hydroxymethylglutaryl-CoA synthase-1	HMGCs1	1.03 ± 0.11	1.60 ± 0.26	4.56 ± 0.73*‡†
Hydroxymethylglutaryl-CoA reductase	HMGCr	0.99 ± 0.13	1.22 ± 0.32	2.93 ± 0.44*†
Apolipoprotein A-1	ApoA1	0.93 ± 0.09	1.26 ± 0.21	0.61 ± 0.11*‡†

All results are expressed as the relative fold change compared to the low-fat control diet group ± SD ($n = 6$ per each group).
* Significantly different from the corresponding control group with the same dietary composition; $p < 0.05$.
‡ Significantly different from the low-fat diet with the same dietary lipid as a source; $p < 0.05$.
† Significantly different from low-fat control diet group; $p < 0.05$.

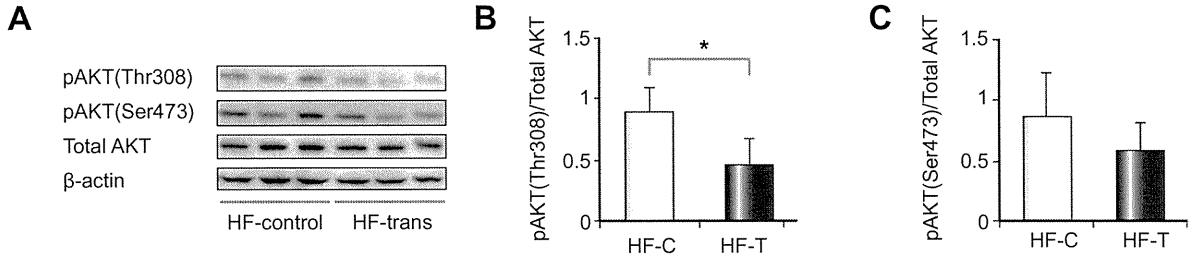

Fig. 3. Effect of excessive TFA consumption of AKT in the high-fat diet-fed mice liver. (A) Representative pictures of phospho-AKT (Thr308 and Ser473), total AKT and β-actin Western blots as well as densitometric analysis of the (B) pAKT(Thr308) or (C) pAKT(Thr473)/total AKT ratio. *p <0.05.

though a few studies have reported that hepatic steatosis [30] and ALT elevation [17] were induced by a TFA-rich diet in mice, the mechanisms remain to be clarified. In agreement with this, the HF-T group showed severe steatosis with a significant transaminase elevation, while HF-C-fed mice only showed moderate steatosis without liver injury, in addition we showed that relatively small amounts of TFA-rich oil intake do not induce severe steatosis and liver injury in the current study. Interestingly, the plasma cholesterol fraction was significantly altered even in the LF-T group in association with the elevation of the total: HDL-cholesterol ratio, a risk factor index of coronary artery disease [22]. The alteration of the plasma cholesterol fraction might be partially explained by changes in the cholesterol metabolism-related gene expressions in the HF-T group, but not in the LF-T group. We could not determine why the cholesterol fraction was altered in the LF-T group, but it might be partially due to the modified membrane fluidity induced by TFA intake [14]. That a relatively small TFA intake could affect the cholesterol fraction but not the liver might be the reason why less attention has been paid to the liver until recently.

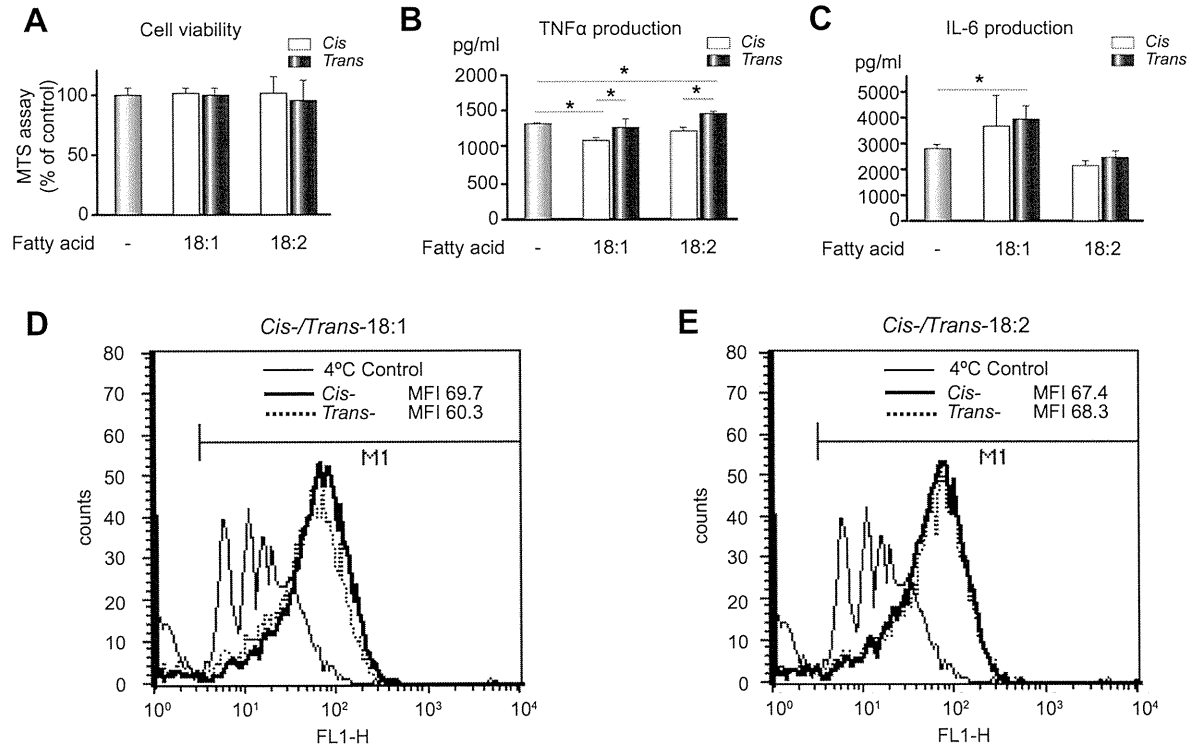

Fig. 4. The impact of *cis*-/*trans*-fatty acid on the cytokine production and phagocytotic ability of KCs. (A) No fatty acids (200 μM) shows cytotoxicity for primary KCs after 24 h incubation, but (B) increases TNFα production in both C18:1 and C18:2-TFA-containing medium compared to its *cis*-structural isomer. (D) IL-6 production increases in C18:1-containing medium and remains unchanged in C18:2-containing medium, whereas the *cis*- or *trans*-structural difference does affect the results. The influence of the C18:1 (D) and C18:2 (E) *cis*-/*trans*-fatty acid on the phagocytotic ability of KCs is measured by flow cytometry analysis. MFI: mean fluorescence intensity (n = 8 for each group, A–C). *p <0.05.

One of the noted biochemical changes seen in the HF-T group was the elevation of plasma FFA, almost all of which is derived from adipose tissue and accumulates in the liver as TG in a dose-dependent fashion [7]. The increase of plasma FFA might be due to the TFA incorporation in the adipocyte plasma membrane resulting in decreased membrane fluidity, accompanied by increased adipose tissue insulin resistance as evidenced by increased lipolysis, decreased antilipolysis and decreased glucose uptake in rat adipocytes [14]. In addition, in contrast to TG, the circulating FFAs [21] and accumulation of FFAs in liver [32] are known to exert lipotoxicity to hepatocytes, so the significant increase of the plasma FFA in the HF-T group might affect the pathophysiology. On the other hand, hepatic FFA was higher in HF than LF irrespective of the dietary lipid sources, and it was reported that forced high-fat feeding induced NASH in mice, while usual high-fat intake does not [6]. Hepatic FFA accumulation remained unaltered among healthy, NAFLD and NASH subjects liver [24], so it might not be necessary for the progression to NASH but could be a exacerbating factor in the case of excess fat consumption. Therefore, elevated plasma FFA and accumulated hepatic lipid peroxide [23] would contribute synergistically to the liver injury in this model.

A previous study reported that TFA intake decreased the arachidonic acid level and induced insulin resistance in adipose tissue, probably due to the decreased membrane fluidity [14], and the present study also revealed a decrease of the arachidonic acid level in the liver and lower phosphorylation status of AKT which could reflect the hepatic insulin resistant status in the HF-T group. In addition, a human lipidomic analysis of NAFLD/NASH liver described a decrease of arachidonic acid and unaltered levels of precursor linoleic acid, but the study did not address TFA consumption [24]. Although, the mechanisms of the arachidonic acid decrease and involvement in the insulin resistance and progression to NASH remain to be clarified, these common findings might suggest that TFA intake influences both the liver and adipose tissue in a somewhat similar fashion in NASH patients and people who consume excess TFAs.

Typical pathological findings in human NAFLD/NASH patients such as macrovesicular lipid deposit and inflammation are usually identified around zone 3, though the mice liver showed lipid deposits around zone 1 even in the control lipid-fed group. Microvesicular lipid droplets were remarkable in the HF-T group, so it might be difficult to assess the pathological changes using a human scoring system such as NAS. The pathological differences might be due to a specific problem, since the pediatric NAFLD is known to show histological findings around zone 1 [26], which might be related to the dietary habit of consuming excess TFAs from snacks and first food.

Although the expression of proinflammatory cytokines such as TNFα [30] and IL-1β [17] have been shown to be induced in the mice liver by TFA-rich diets, this was not the case in the current study. However, a previous study reported that, among hypercholesterolemic subjects, the production of TNFα by cultured mononuclear cells was increased by a TFA-rich soy bean margarine diet compared with a natural soybean oil diet [12], and we showed KCs increased TNFα production in TFA-containing medium compared to that of *cis*-structural isomer-containing medium. Accordingly, pathophysiological conditions induced by TFA consumption could be partially due to alterations in the monocyte/macrophage ability in proinflammatory cytokine production and phagocytosis, and KCs in particular may play important roles in the local circumstances.

With regard to the adipokines, the adiponectin levels were not changed between the HF-C and HF-T group, but plasma leptin was significantly increased in the HF-T group. Leptin is an appetite-suppressing and body weight-regulating adipokine, and is even related to liver regeneration and fibrosis [13]; hyperleptinemia might be related directly to the elevation of type1 collagen α1 mRNA expression in the liver.

In terms of the severe steatosis of the model, the lipogenetic genes such as FAS, ACC, SREBP-1 and PPARγ2 were coordinately induced, but PGC-1β was not. PGC-1β is known to be induced in the liver by short term high-fat feeding, to coactivate SREBP-1, but to reduce hepatic fat accumulation. However, since it was not investigated in this study, the decrease of PGC-1β gene expression might be due to long term feeding or any other factors, such as the relatively low carbohydrate diet. It was reported that a TFA-rich diet suppressed the PPARγ gene expression in rat adipose tissue [8], and that lipogenic gene expressions in the liver and the adipose tissue are reciprocal modulations [4], which might reflect the core mechanisms of the heterotopic fat accumulation *in vivo*.

In summary, excess TFA consumption induces significant hepatic steatosis accompanied by augmentation of the hepatic lipogenic gene expressions, FFA influx into the liver, and the hepatic accumulation of lipid peroxide. The hepatic accumulation of TFA and the reduction of the arachidonic acid content were the lipidomic properties in this model. Together with their potential induction of local cytokines by KCs, lipid species including TFA may play a pivotal role in the development of non-alcoholic fatty liver diseases.

Acknowledgements

This study was supported in part from Health and Labour Sciences Research Grants for the Research on Measures for Intractable Diseases (from the Ministry of Health, Labour and Welfare of Japan), from Grant-in-Aid for Scientific Research C (20590755 to KF) from Japanese Society of Promotion of Science (JSPS).

Conflicts of interest

The authors who have taken part in this study declared that they do not have anything to disclose regarding funding or conflict of interest with respect to this manuscript.

Supplementary data

Supplementary data associated with this article can be found, in the online version, at doi:10.1016/j.jhep.2010.02.029.

References

[1] Babior BM. Oxygen-dependent microbial killing by phagocytes (first of two parts). N Engl J Med 1978;298:659–668.
[2] Browning JD, Szczepaniak LS, Dobbins R, Nuremberg P, Horton JD, Cohen JC, et al. Prevalence of hepatic steatosis in an urban population in the United States: impact of ethnicity. Hepatology 2004;40:1387–1395.
[3] Buettner R, Parhofer KG, Woenckhaus M, Wrede CE, Kunz-Schughart LA, Scholmerich J, et al. Defining high-fat-diet rat models: metabolic and molecular effects of different fat types. J Mol Endocrinol 2006;36:485–501.
[4] Cao H, Gerhold K, Mayers JR, Wiest MM, Watkins SM, Hotamisligil GS. Identification of a lipokine, a lipid hormone linking adipose tissue to systemic metabolism. Cell 2008;134:933–944.

[5] Day CP, James OF. Steatohepatitis: a tale of two "hits"? Gastroenterology 1998;114:842–845.
[6] Deng QG, She H, Cheng JH, French SW, Koop DR, Xiong S, et al. Steatohepatitis induced by intragastric overfeeding in mice. Hepatology 2005;42:905–914.
[7] Donnelly KL, Smith CI, Schwarzenberg SJ, Jessurun J, Boldt MD, Parks EJ. Sources of fatty acids stored in liver and secreted via lipoproteins in patients with nonalcoholic fatty liver disease. J Clin Invest 2005;115:1343–1351.
[8] Duque-Guimaraes DE, de Castro J, Martinez-Botas J, Sardinha FL, Ramos MP, Herrera E, et al. Early and prolonged intake of partially hydrogenated fat alters the expression of genes in rat adipose tissue. Nutrition 2009;25: 782–789.
[9] Farrell GC, Larter CZ. Nonalcoholic fatty liver disease: from steatosis to cirrhosis. Hepatology 2006;43:S99–S112.
[10] Folch J, Lees M, Sloane Stanley GH. A simple method for the isolation and purification of total lipides from animal tissues. J Biol Chem 1957;226: 497–509.
[11] Gonzalez-Periz A, Horrillo R, Ferre N, Gronert K, Dong B, Moran-Salvador E, et al. Obesity-induced insulin resistance and hepatic steatosis are alleviated by omega-3 fatty acids: a role for resolvins and protectins. FASEB J 2009;23:1946–1957.
[12] Han SN, Leka LS, Lichtenstein AH, Ausman LM, Schaefer EJ, Meydani SN. Effect of hydrogenated and saturated, relative to polyunsaturated, fat on immune and inflammatory responses of adults with moderate hypercholesterolemia. J Lipid Res 2002;43:445–452.
[13] Honda H, Ikejima K, Hirose M, Yoshikawa M, Lang T, Enomoto N, et al. Leptin is required for fibrogenic responses induced by thioacetamide in the murine liver. Hepatology 2002;36:12–21.
[14] Ibrahim A, Natrajan S, Ghafoorunissa R. Dietary trans-fatty acids alter adipocyte plasma membrane fatty acid composition and insulin sensitivity in rats. Metabolism 2005;54:240–246.
[15] Kechagias S, Ernersson A, Dahlqvist O, Lundberg P, Lindstrom T, Nystrom FH. Fast-food-based hyper-alimentation can induce rapid and profound elevation of serum alanine aminotransferase in healthy subjects. Gut 2008;57:649–654.
[16] Kleiner DE, Brunt EM, Van Natta M, Behling C, Contos MJ, Cummings OW, et al. Design and validation of a histological scoring system for nonalcoholic fatty liver disease. Hepatology 2005;41:1313–1321.
[17] Koppe SW, Elias M, Moseley RH, Green RM. Trans fat feeding results in higher serum alanine aminotransferase and increased insulin resistance compared with a standard murine high-fat diet. Am J Physiol Gastrointest Liver Physiol 2009;297:G378–G384.
[18] Larter CZ, Yeh MM, Haigh WG, Williams J, Brown S, Bell-Anderson KS, et al. Hepatic free fatty acids accumulate in experimental steatohepatitis: role of adaptive pathways. J Hepatol 2008;48:638–647.
[19] Lin J, Yang R, Tarr PT, Wu PH, Handschin C, Li S, et al. Hyperlipidemic effects of dietary saturated fats mediated through PGC-1beta coactivation of SREBP. Cell 2005;120:261–273.
[20] Lopez-Garcia E, Schulze MB, Meigs JB, Manson JE, Rifai N, Stampfer MJ, et al. Consumption of trans fatty acids is related to plasma biomarkers of inflammation and endothelial dysfunction. J Nutr 2005;135:562–566.
[21] Malhi H, Gores GJ. Molecular mechanisms of lipotoxicity in nonalcoholic fatty liver disease. Semin Liver Dis 2008;28:360–369.
[22] Mensink RP, Zock PL, Kester AD, Katan MB. Effects of dietary fatty acids and carbohydrates on the ratio of serum total to HDL cholesterol and on serum lipids and apolipoproteins: a meta-analysis of 60 controlled trials. Am J Clin Nutr 2003;77:1146–1155.
[23] Milagro FI, Campion J, Martinez JA. Weight gain induced by high-fat feeding involves increased liver oxidative stress. Obesity (Silver Spring) 2006;14: 1118–1123.
[24] Puri P, Baillie RA, Wiest MM, Mirshahi F, Choudhury J, Cheung O, et al. A lipidomic analysis of nonalcoholic fatty liver disease. Hepatology 2007;46:1081–1090.
[25] Reid AE. Nonalcoholic steatohepatitis. Gastroenterology 2001;121:710–723.
[26] Schwimmer JB, Behling C, Newbury R, Deutsch R, Nievergelt C, Schork NJ, et al. Histopathology of pediatric nonalcoholic fatty liver disease. Hepatology 2005;42:641–649.
[27] Shimano H, Horton JD, Hammer RE, Shimomura I, Brown MS, Goldstein JL. Overproduction of cholesterol and fatty acids causes massive liver enlargement in transgenic mice expressing truncated SREBP-1a. J Clin Invest 1996;98:1575–1584.
[28] Su GL, Klein RD, Aminlari A, Zhang HY, Steinstraesser L, Alarcon WH, et al. Kupffer cell activation by lipopolysaccharide in rats: role for lipopolysaccharide binding protein and toll-like receptor 4. Hepatology 2000;31: 932–936.
[29] Sun Q, Ma J, Campos H, Hankinson SE, Manson JE, Stampfer MJ, et al. A prospective study of trans fatty acids in erythrocytes and risk of coronary heart disease. Circulation 2007;115:1858–1865.
[30] Tetri LH, Basaranoglu M, Brunt EM, Yerian LM, Neuschwander-Tetri BA. Severe NAFLD with hepatic necroinflammatory changes in mice fed trans fats and a high-fructose corn syrup equivalent. Am J Physiol Gastrointest Liver Physiol 2008;295:G987–G995.
[31] Tsuzuki T, Tokuyama Y, Igarashi M, Nakagawa K, Ohsaki Y, Komai M, et al. Alpha-eleostearic acid (9Z11E13E-18:3) is quickly converted to conjugated linoleic acid (9Z11E-18:2) in rats. J Nutr 2004;134:2634–2639.
[32] Yamaguchi K, Yang L, McCall S, Huang J, Yu XX, Pandey SK, et al. Inhibiting triglyceride synthesis improves hepatic steatosis but exacerbates liver damage and fibrosis in obese mice with nonalcoholic steatohepatitis. Hepatology 2007;45:1366–1374.
[33] Zhang YL, Hernandez-Ono A, Siri P, Weisberg S, Conlon D, Graham MJ, et al. Aberrant hepatic expression of PPARgamma2 stimulates hepatic lipogenesis in a mouse model of obesity, insulin resistance, dyslipidemia, and hepatic steatosis. J Biol Chem 2006;281:37603–37615.

Adenosine Triphosphate Release and Purinergic (P2) Receptor–Mediated Secretion in Small and Large Mouse Cholangiocytes

Kangmee Woo,[1] Meghana Sathe,[1] Charles Kresge,[1] Victoria Esser,[2] Yoshiyuki Ueno,[5] Julie Venter,[3] Shannon S. Glaser,[3] Gianfranco Alpini,[3,4] and Andrew P. Feranchak[1]

Adenosine triphosphate (ATP) is released from cholangiocytes into bile and is a potent secretogogue by increasing intracellular Ca^{2+} and stimulating fluid and electrolyte secretion via binding purinergic (P2) receptors on the apical membrane. Although morphological differences exist between small and large cholangiocytes (lining small and large bile ducts, respectively), the role of P2 signaling has not been previously evaluated along the intrahepatic biliary epithelium. The aim of these studies therefore was to characterize ATP release and P2-signaling pathways in small (MSC) and large (MLC) mouse cholangiocytes. The findings reveal that both MSCs and MLCs express P2 receptors, including P2X4 and P2Y2. Exposure to extracellular nucleotides (ATP, uridine triphosphate, or 2′,3′-O-[4-benzoyl-benzoyl]-ATP) caused a rapid increase in intracellular Ca^{2+} concentration and in transepithelial secretion (I_{sc}) in both cell types, which was inhibited by the Cl^- channel blockers 5-nitro-2-(-3-phenylpropylamino)-benzoic acid (NPPB) or niflumic acid. In response to mechanical stimulation (flow/shear or cell swelling secondary to hypotonic exposure), both MSCs and MLCs exhibited a significant increase in the rate of exocytosis, which was paralleled by an increase in ATP release. Mechanosensitive ATP release was two-fold greater in MSCs compared to MLCs. ATP release was significantly inhibited by disruption of vesicular trafficking by monensin in both cell types. *Conclusion:* These findings suggest the existence of a P2 signaling axis along intrahepatic biliary ducts with the "upstream" MSCs releasing ATP, which can serve as a paracrine signaling molecule to "downstream" MLCs stimulating Ca^{2+}-dependent secretion. Additionally, in MSCs, which do not express the cystic fibrosis transmembrane conductance regulator, Ca^{2+}-activated Cl^- efflux in response to extracellular nucleotides represents the first secretory pathway clearly identified in these cholangiocytes derived from the small intrahepatic ducts. (HEPATOLOGY 2010;52:1819-1828)

Cholangiocytes, the epithelial cells that form the intrahepatic bile ducts, represent an important component of the bile secretory unit. Although bile formation is initiated at the hepatocyte canalicular membrane, cholangiocytes subsequently modify the composition of bile through regulated ion secretion throughout the network of bile ducts.[1] Interestingly, secretory mechanisms along the intrahepatic bile ducts are not uniform. In all biliary models studied, including human, rat, and mouse bile ducts, cholangiocytes are known to be morphologically and functionally heterogeneous. Large cholangiocytes, from large ducts, express secretin receptors on the basolateral membrane and express cystic fibrosis transmembrane

Abbreviations: AE2, anion exchanger 2; ATP, adenosine triphosphate; Bz-ATP, 2′,3′-O-(4-benzoyl-benzoyl)-ATP; cAMP, cyclic adenosine monophosphate; CFTR, cystic fibrosis transmembrane conductance regulator; fura-2-AM, fura-2-acetoxymethyl ester; IP3, inositol 1,4,5-triphosphate; Isc, transepithelial short-circuit current response; MLC, mouse large cholangiocyte; MSC, mouse small cholangiocyte; NPPB, 5-nitro-2-(-3-phenylpropylamino)-benzoic acid; RT-PCR, reverse transcription polymerase chain reaction; UTP, uridine triphosphate.

From the [1]Department of Pediatrics, and [2]Internal Medicine, University of Texas Southwestern Medical Center, Dallas, TX; [3]Research, Central Texas Veterans Health Care System, Scott & White Digestive Disease Research Center, Scott & White Healthcare, Temple, TX; [4]Department of Medicine, Division Gastroenterology, Texas A&M Health Science Center College of Medicine, Temple, TX; and [5]Tohoku University, School of Medicine, Sendai, Japan.

Received September 21, 2009; accepted July 22, 2010.

This study was supported by the Cystic Fibrosis Foundation (FERANC08G0), the Children's Medical Center Foundation, and the National Institute of Diabetes, Digestive and Kidney Diseases (NIDDK) of the National Institutes of Health, grants DK078587 (to A.P.F.) and DK054811 (to G.A.), and a VA Merit Award (to G.A.).

conductance regulator (CFTR) and the HCO_3^-/Cl^- anion exchanger 2 (AE2) on the apical membrane,[2-4] and hence respond to secretin with an increase in [cAMP] (intracellular cyclic adenosine monophosphate concentration), and subsequent Cl^- and HCO_3^- efflux into the lumen. Conversely, small cholangiocytes, from small ducts, do not express secretin receptors, CFTR, or HCO_3^-/Cl^- exchanger and do not exhibit a secretory response to secretin.[3] In human liver, parallel to the findings observed in the rat and mouse, secretin-stimulated duct secretory activity is heterogeneous, because only medium and large interlobular bile ducts express the Cl^-/HCO_3^- exchanger AE2.[5]

Recently, secretion mediated by extracellular nucleotides (e.g., adenosine triphosphate [ATP]) acting on purinergic (P2) receptors on the luminal membrane of biliary epithelial cells has emerged as functionally important. ATP is present in bile,[6] and binding of ATP to P2 receptors increases K^+,[7,8] and Cl^- efflux from isolated cholangiocytes[9,10] and dramatically increases transepithelial secretion in biliary epithelial monolayers.[10,11] Indeed, the magnitude of the secretory response to ATP is two-fold to three-fold greater than that to cAMP.[10] Interestingly, recent evidence suggests that even cAMP-stimulated bile flow is mediated by ATP release into the duct lumen and stimulation of apical P2 receptors.[12] Together, these studies challenge and extend the conventional model that centers on the concept that cAMP-dependent opening of CFTR-related Cl^- channels is the driving force for cholangiocyte secretion. Rather, the operative regulatory pathways appear to take place within the lumen of intrahepatic ducts, where release of ATP into bile is a final common pathway controlling ductular bile formation. In light of recent studies demonstrating that the mechanical effects of fluid-flow or shear stress at the apical membrane of biliary epithelial cells is a robust stimulus for ATP release,[13] a model emerges in which mechanosensitive ATP release and Cl^- secretion is a dominant pathway regulating biliary secretion.

Although cholangiocytes express a repertoire of both P2X and P2Y receptors,[11,14,15] it is unknown if expression differs between small and large cholangiocytes and/or if functional differences exist in ATP release and signaling along the bile duct. The aim of the current studies therefore was to determine if a potential P2 signaling axis may exist along the bile duct by evaluating mechanosensitive ATP release and exocytosis, P2 receptor expression and function, and secretion mediated by extracellular nucleotides in both small (MSC) and large (MLC) mouse cholangiocytes.

Materials and Methods

Cell Models. Studies were performed in mouse cholangiocytes isolated from normal mice (BALB/c) and immortalized by transfection with the simian virus 40 large-T antigen gene.[4] These cells demonstrate identical properties to freshly isolated small and large mouse cholangiocytes.[3] Cells were maintained in culture as described.[3,4] Additional studies of P2 receptor expression were performed in primary cholangiocytes isolated from C57BL/6 mice (Charles River, Wilmington, MA) as previously described.[16,17] All animal experiments were performed in accordance with a protocol approved by the Scott & White Institutional Animal Care and Use Committee and in accordance with the Guide for the Care and Use of Laboratory Animals published by the U.S. National Institutes of Health (NIH Publication No. 85-23, revised 1996).

Total RNA Isolation and RT-PCR Analysis. Total RNA was extracted using TRIZOL Reagent (Invitrogen, Carlsbad, CA) and 1 μg RNA was reverse transcribed in the presence of 100 pmol oligo-deoxythymidine primer. For reverse transcription polymerase chain reaction (RT-PCR), aliquots of 5% of the total complementary DNA were amplified with TaqDNA polymerase in a reaction mixture containing 20 pmol of 5′ and 3′ primers specifically designed for various P2X and P2Y receptors (Supporting Information Methods and Supporting Information Table 1).

Measurement of Intracellular Ca^{2+} Concentration. MLCs and MSCs were grown to confluence on coverglass (Fig. 2), loaded with 2.5 μg/mL of fura-2-acetoxymethyl ester (fura-2-AM; TEF Laboratories, Austin, TX), placed in a perfusion chamber (RC-25F/PHA; Warner Instruments) on the stage of an inverted fluorescence microscope (Nikon TE2000), and the inflow and outflow ports were connected to a syringe pump. Changes of $[Ca^{2+}]_i$ (the intracellular calcium

Address reprint requests to: Andrew P. Feranchak, M.D., UT Southwestern Medical Center, 5323 Harry Hines Boulevard, Dallas, TX 75390-9063. E-mail: drew.feranchak@UTSouthwestern.edu; fax: 214-648-2673.

View this article online at wileyonlinelibrary.com.

DOI 10.1002/hep.23883

Potential conflict of interest: Nothing to report.

Additional Supporting Information may be found in the online version of this article.

concentration) were measured at excitation wavelength of 340 nm (calcium-bound fura-2-AM) and 380 nm (calcium-free fura-2-AM), and emission wavelength of 510 nm and $[Ca^{2+}]_i$ was calculated.

Immunostaining. Confluent MSCs and MLCs were incubated with acetylated α-tubulin antibody (Sigma), as a marker for the primary cilium, and rhodamine phalloidin (Invitrogen) to label actin. Imaging was performed using a PerkinElmer UltraVIEW ERS spinning disk confocal microscope (PerkinElmer, Boston, MA). Imaris 5.0 (Bitplane, Inc., Saint Paul, MN) was used for three-dimensional volume rendering of z-stacks.

Measurement of Exocytosis. Exocytosis was assessed by real time imaging using the fluorescent dye FM1-43 (Molecular Probes, Inc., Eugene, OR) as previously described.[18] FM1-43 is weakly fluorescent in aqueous solution, but its fluorescence increases >300-fold when it binds plasma membrane and, therefore, it is a useful dye for the measurement of increased plasma membrane due to fusion of vesicle membrane with the plasma membrane during exocytosis.

Measurement of ATP Release. Bulk ATP release was studied from confluent cells using the luciferin-luciferase (L-L) assay as previously described.[13,19,20] Cell swelling was induced by adding water to dilute media 33% and defined shear stress was applied to confluent cells in a parallel plate chamber. All luminescence values are reported as relative change from basal luminescence per total protein level in the sample (measured in micrograms per milliliter) to control for any potential differences in luciferase activity or confluency between samples, respectively. Detailed protocols for measurements of ATP release, ATP degradation, protein levels, and lactate dehydrogenase are described in Supporting Information Methods.

Transepithelial Cl− Secretion. MLCs and MSCs were grown on collagen-coated polycarbonate filters with a pore size of 0.4 μm (Costar, Cambridge, MA) and the transmembrane resistance was measured daily (Evohm voltmeter; World Precision Instruments, Sarasota, FL).[21] Filters were mounted in an Ussing chamber, filled with standard buffer solution, and transepithelial short-circuit current response (I_{sc}) was measured under 0 mV voltage-clamp conditions through agar bridges connected to Ag-AgCl electrodes using an epithelial voltage clamp amplifier (model EC-825; Warner Instruments, MRA International, Naples, FL). The I_{sc} represents the net sum of the transepithelial fluxes of anion and cation and the level of ion secretion.[11] Studies included paired, same-day monolayers to minimize any potential effects of day-to-day variability.

Reagents and Statistics. Detailed descriptions of the reagents, buffer solutions, experimental protocols, and statistical analysis are provided in Supporting Information Materials.

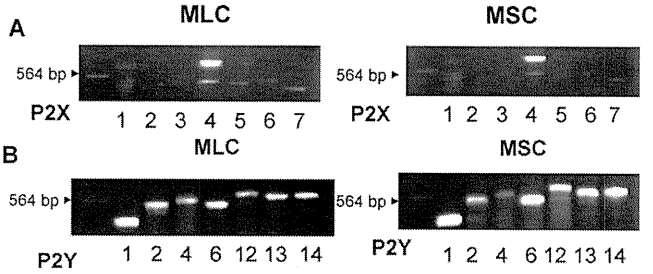

Fig. 1. Mouse cholangiocytes express P2 receptors. Molecular expression of P2X and P2Y receptor subtypes was evaluated by RT-PCR with specific oligonucleotides. (A) P2X receptor expression. P2X4 is the predominant P2X receptor in both mouse large (MLC), left panel, and mouse small (MSC), right panel, cholangiocytes. (B) P2Y receptor expression. Both MLCs and MSCs express multiple P2Y receptor subtypes, including P2Y1, P2Y2, P2Y4, P2Y6, P2Y12, P2Y13, and P2Y14. The arrowhead indicates a 564-base pair (bp) λDNA-Hind III fragment.

Results

Large and Small Cholangiocytes Express a Repertoire of P2X and P2Y Receptors. In both MLCs and MSCs, complementary DNAs were probed with oligonucleotide primers specific to the seven P2X subtypes and seven P2Y subtypes in mouse (shown in Supporting Information Table 1) and amplified using RT-PCR. Representative studies are shown in MLCs and MSCs (Fig. 1), and in primary isolated cholangiocytes (Supporting Information Fig. 1). In both MLCs and MSCs, clear bands corresponding to P2X4 and all seven P2Y receptors (P2Y1, P2Y2, P2Y4, P2Y6, P2Y11, P2Y12, and P2Y13) are present. These results are consistent with previous studies of human and rat biliary cells where a predominance of P2X4 and multiple P2Y receptors were observed.[11,14,15]

Agonist Profile of Nucleotide-Stimulated Ca^{2+} Fluorescence. To establish the functional significance of mouse cholangiocyte P2 receptor expression, MSCs and MLCs were grown to confluence (Fig. 2) and changes in Ca^{2+} fluorescence measured in response to P2Y and P2X agonists. Exposure to ATP, UTP, a P2Y-preferring agonist, or Bz-ATP, a P2X-preferring agonist, all resulted in significant increases in $[Ca^{2+}]_i$ in both MLCs and MSCs (Fig. 3). The ATP-stimulated increase in $[Ca^{2+}]_i$ was abolished by the P2Y receptor blocker, suramin (Fig. 3D). Together, these results demonstrate that P2X4 and P2Y receptors expressed by both MLCs and MSCs are functionally active. No differences were observed between MLCs and MSCs in either the magnitude or kinetics of the Ca^{2+} response to any of the nucleotides.

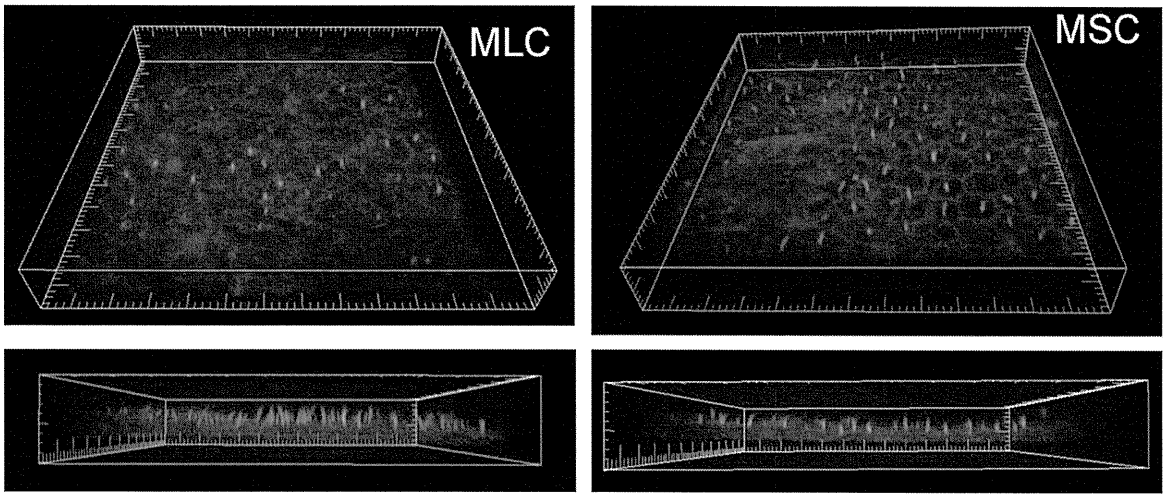

Fig. 2. MLCs and MSCs form polarized monolayers. MLCs (left) and MSCs (right) were cultured on coverglass for 5 days and stained for acetylated α-tubulin, as a cilia marker protein (green), and phalloidin, for actin localization (red). Bottom panels represent *z* axis to highlight cilia. Scale, small hatch marks = 5 μm.

Functional Role for P2 Receptors in Transepithelial Secretion. When cultured as described, both MSCs and MLCs developed an increase in transmembrane resistance by day 3 signifying the development of confluent monolayers with tight junctions (Fig. 4A). When mounted in an Ussing chamber, confluent MLCs and MSCs monolayers exhibited a basal I_{sc}, reflecting transepithelial secretion, which increased dramatically in response to the addition of ATP (100 μM) to the apical chamber (Fig. 4B,C). The nucleotide-stimulated I_{sc} was significantly inhibited by the nonspecific Cl^- channel blocker, 5-nitro-2-(-3-phenylpropylamino)-benzoic acid (NPPB), or by the Ca^{2+}-activated Cl^- channel blocker niflumic acid (Fig. 4C,F). Additionally, preincubation with the IP3 receptor blocker, 2-APB, significantly inhibited the ATP-stimulated increase in I_{sc} in both MLC and MSC (Fig. 4C). In separate experiments, the effect of apical versus basolateral P2 receptor stimulation on the I_{sc} was determined. For both MSCs and MLCs, an increase in the I_{sc} was observed when nucleotides were added to either chamber, consistent with functional expression of P2 receptors on both apical and basolateral membranes. The magnitude of the change in I_{sc} was similar

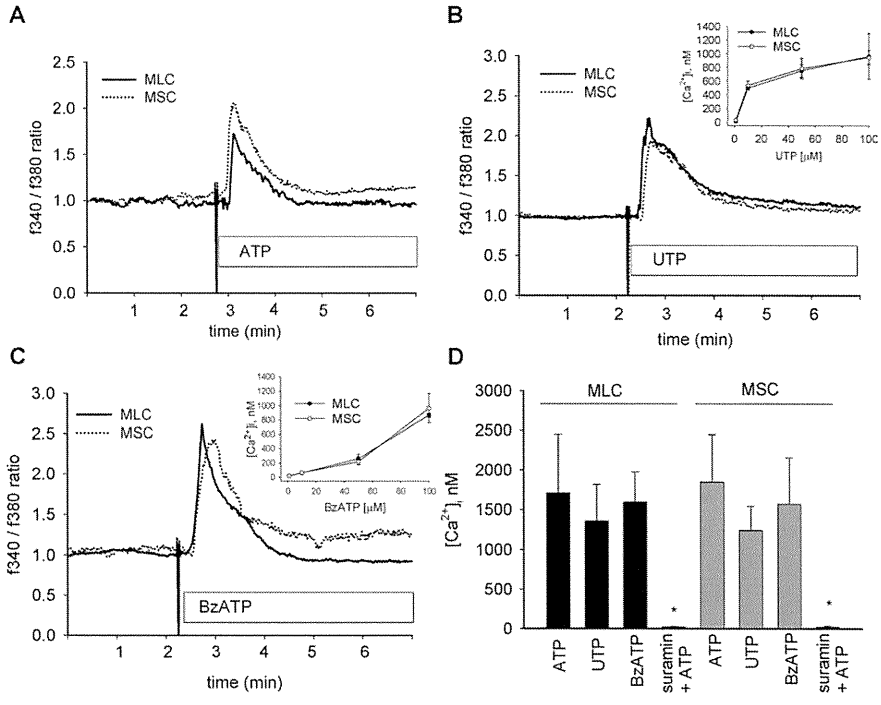

Fig. 3. P2 receptor agonists increase intracellular Ca^{2+} in mouse cholangiocytes. MLCs and MSCs were loaded with fura-2-AM and exposed to extracellular nucleotides, ATP (100 μM), UTP (100 μM), or Bz-ATP (100 μM) as indicated. The *y* axis values represent the ratio of fluorescence at 340 (f340) and at 380 nm (f380). (A-C) Representative studies. The Ca^{2+} fluorescence increased rapidly in both MLCs (solid line) and MSCs (dotted line) upon exposure to nucleotides. Insets in (B) and (C) demonstrate dose-response for respective agonist. (D) Cumulative data. Values represent the maximal $[Ca^{2+}]_i$ in nM. $[Ca^{2+}]_i$ was calculated based on maximal and minimal Ca^{2+} fluorescence obtained by exposure to ionomycin (5 μM) and EGTA (10 mM), respectively (N = 3-6 each). *Suramin significantly inhibits ATP-stimulated $[Ca2+]_i$, $P < 0.05$.

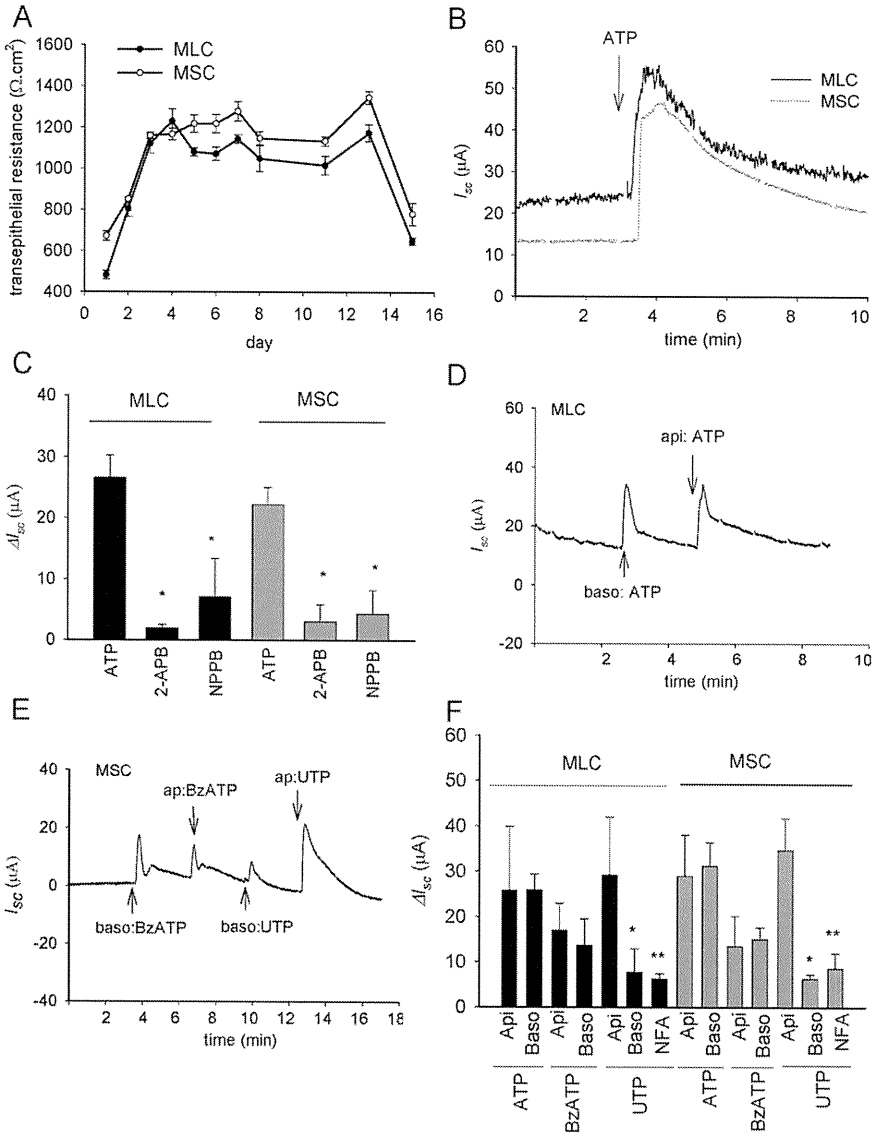

Fig. 4. Mouse cholangiocytes form polarized monolayers and exhibit increases in transepithelial Cl^- secretion in response to extracellular nucleotides. (A) Transmembrane resistance ($\Omega.cm^2$) was measured at the time points indicated in MLCs and MSCs grown on semipermeable filters. (B) Representative tracings of MLCs or MSCs mounted in an Ussing chamber. The *y* axis represents short-circuit current (I_{sc}) across monolayers measured under voltage-clamp conditions (μA). ATP (100 μM), added to the apical chamber, significantly increased I_{sc}. (C) Cumulative data demonstrating effect of 2-APB or NPPB on ATP-stimulated I_{sc}. The *y* axis values are reported as ΔI_{sc} (maximum I_{sc} – basal I_{sc}). *The 2-APB or NPPB significantly inhibit ATP-stimulated ΔI_{sc} ($P < 0.05$, n= 3-9 each). (D) Representative recording of apical or basolateral additions of ATP (100 μM)-stimulated I_{sc} in MLCs. (E) Representative recording of apical or basolateral additions of BzATP (100 μM) and UTP (100 μM) in MSCs. (F) Cumulative data. Values (mean ± standard error of the mean [SEM]) represent Δ I_{sc}. Apical addition (Api) and basolateral addition (Baso), of respective reagent (n = 4-12 each). *Apical addition of UTP increases I_{sc} > than basolateral addition ($P < 0.05$). **Niflumic acid (NFA, 250 μM) inhibits UTP-stimulated I_{sc} ($P < 0.05$).

when nucleotides were added to either apical or basolateral compartments for all nucleotides tested except for UTP which caused a significantly greater increase in I_{sc} when added apically versus basolateral addition. Thus, both MSCs and MLCs express functional P2 receptors on both apical and basolateral membranes. Nucleotide binding to P2 receptors causes an increase in $[Ca^{2+}]_i$, predominantly through an IP3 receptor-dependent mechanism, which stimulates Ca^{2+}-activated Cl^- channels, and results in transepithelial secretion. To our knowledge, these represent the first integrated I_{sc} measurements of transepithelial secretion in mouse cholangiocytes. Furthermore, in MSC, which do not express CFTR, Ca^{2+}-activated Cl^- efflux in response to extracellular nucleotides represents the first secretory pathway clearly identified in these cells derived from the small intrahepatic ducts.

Mechanosensitive ATP Release. In human biliary cells and normal rat cholangiocyte monolayers, mechanical stimulation,[22] shear stress,[13] and cell swelling secondary to hypotonic exposure,[22] have all been identified as significant stimuli for ATP release. Studies were performed to determine if these mechanical stimuli result in a similar increase in the magnitude of ATP release in mouse cholangiocytes. First, in response to hypotonic exposure (33% dilution) to stimulate cell swelling, a rapid and large increase in ATP release was observed in both MLCs and MSCs (Fig. 5A). The magnitude of the response, which peaked within 30 seconds, was significantly greater in MSCs versus MLCs (Fig. 5A,C). Separate studies were performed to assess the effects of shear on ATP release. Under low shear conditions (shear 0.08 dyne/cm^2) no increase in ATP release was observed; however, increasing shear to

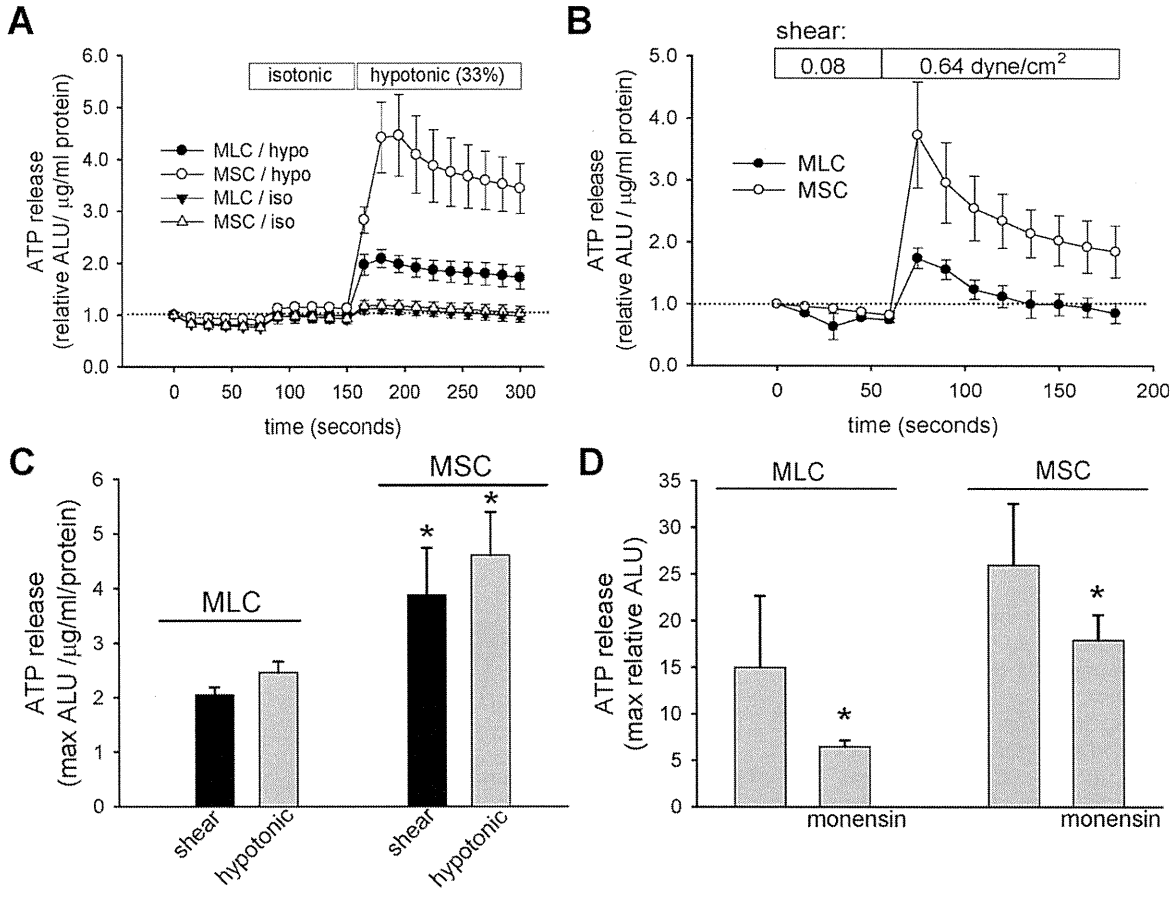

Fig. 5. Mechanosensitive ATP release from mouse cholangiocytes. ATP in the extracellular media was detected using the luciferin-luciferase assay and quantified as arbitrary light units (ALU). The *y* axis represents relative increase from basal luminescence (expressed as relative ALU/ µg/mL protein). (A) Cell swelling-induced ATP release from confluent MLCs and MSCs. Addition of isotonic media to cells led to a small increase in luminescence. Dilution of media 33% by the addition of water (indicated by bar) led to an increase in ATP release in both MSCs (open circles) and MLCs (closed circles) much greater than control cells exposed to only a second isotonic exposure. (B) Shear-stimulated ATP release from confluent MLCs (closed circles) and MSCs (open circles) cells. Cells were perfused with Optimem and 60 µL aliquots were taken from the efflux every 30 seconds, added to standard L-L reagent, and immediately placed in the Luminometer for luminescence measurement. Bars along top indicate length of low flow (shear 0.08 dyne/cm^2) and high flow (shear 0.64 dyne/cm^2) exposure. (C) Cumulative data demonstrating relative ATP release from both MLCs and MSCs in response to shear (0.64 dyne/cm^2, black bar) and hypotonic exposure (33% dilution, gray bar). Values represent maximum ATP concentration within 30 seconds of shear or hypotonic exposure, mean ± SEM. *ATP release is significantly greater in MSCs versus MLCs, $P < 0.05$. (D) Inhibition of vesicular trafficking inhibits swelling-induced ATP release in MLCs and MSCs. *Monensin (100 µM × 30 minutes) significantly inhibits ATP release in response to hypotonic exposure (33% dilution); $P < 0.05$, n = 4-6 each.

0.64 dyne/cm^2 caused a rapid relative increase in ATP release in both MLCs and MSCs, and again the magnitude of the peak response was significantly greater in MSCs versus MLCs ($P < 0.05$, Fig. 5B,C). No difference was noted in lactate dehydrogenase measurements before or after stimulus, for either hypotonic or shear exposure, excluding cell lysis as contributing to measured ATP (data not shown). In other biliary models, ATP release has been linked to exocytosis.[18] To determine if exocytosis contributes to ATP release in MLCs and MSCs, studies were performed in the presence or absence of monensin, a carboxylic ionophore known to dissipate the transmembrane pH gradients in Golgi and lysosomal compartments and disrupt vesicular trafficking. In both MLCs and MSCs, monensin significantly inhibited swelling-induced (33% hypotonic exposure) ATP release (Fig. 5D). Thus, both MSCs and MLCs exhibit mechanosensitive ATP release which is dependent on intact vesicular trafficking pathways. Additionally, the magnitude of mechanosensitive ATP release is significantly greater (~two-fold) in MSCs compared to MLCs.

Mechanosensitive Exocytosis. To determine if the difference in ATP release observed between MSCs and MLCs are the result of generalized differences in total cellular exocytosis, rates of exocytosis were measured in response to mechanical stimuli in both cell types. After equilibration with FM1-43, cells were exposed to hypotonic buffer (33%) which was associated with a rapid increase in fluorescence, reflecting an increase in

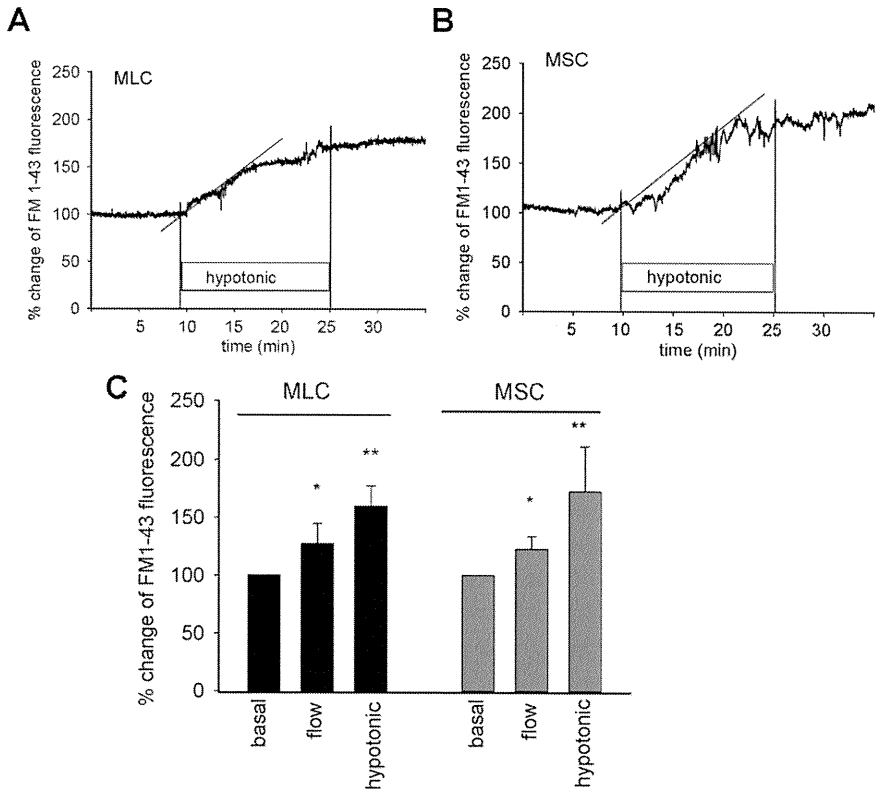

Fig. 6. Mechanosensitive exocytosis. MLCs and MSCs on coverglass were loaded with FM1-43 and exposed to shear or hypotonicity as indicated. The values of the *y* axis represent percent increase in membrane fluorescence. (A,B) Representative figures of swelling-induced exocytosis. FM1-43 fluorescence was stabilized in isotonic buffer before the cells were exposed to hypotonic buffer (33%). Hypotonic exposure rapidly increased plasma membrane fluorescence as a result of vesicular exocytosis in both (A) MLCs and (B) MSCs. Dotted line represents best-fit regression analysis. (E) Cumulative data demonstrating maximum magnitude of exocytosis in both MLCs and MSCs in response to shear (0.64 dyne/cm^2) or hypotonic (33%) exposure. Values represent maximum percent change in FM1-43 fluorescence (n = 5-6 each). *$P < 0.05$ shear versus basal; **$P < 0.05$ hypotonic exposure versus isotonic.

exocytosis (Fig. 6). In separate studies, exposure to shear (0.64 dyne/cm^2) also resulted in an increase in exocytosis (Fig. 6). These findings suggest a functional link between exocytosis and ATP release in both MLCs and MSCs. There was no significant difference noted in the rate or magnitude of exocytosis between MLCs and MSCs in response to either of these mechanical stimuli.

ATP Degradation. The concentration of extracellular ATP in bile is regulated not only through the rate of ATP release, but also through degradation pathways.[23] To determine if differences exist in the kinetics of ATP degradation between MSCs and MLCs, the media bathing confluent cells was loaded with exogenous ATP (10 nM). Changes in bioluminescence were monitored continuously until relative ALU returned to basal levels. As shown in Fig. 7, addition of ATP (10 nM) to MLCs increased relative bioluminescence 2.7-fold. The time course of degradation was described by a single exponential ($y = ae^{-0.038\ min}$, r = 0.99). By comparison, addition of ATP to MSCs increased bioluminescence 2.5-fold with a similar rate of degradation

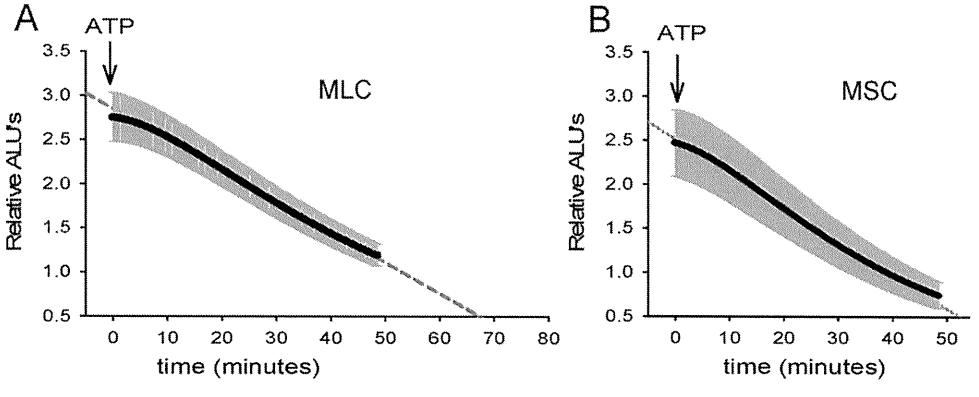

Fig. 7. Kinetics of ATP degradation in mouse cholangiocytes. ATP degradation was assessed after addition of ATP (10 nM, at arrow) to apical membrane of confluent (A) MLCs and (B) MSCs. The *y* axis represents relative arbitrary light units (ALU). Values represent means (black points) ± SEM (gray bars); n = 4 monolayers/time point. Dashed line represents best-fit regression.

described by a single exponential ($y = ae^{-0034\ min}$, r = 0.99). Thus, MLCs and MSCs display functionally similar ATP degradation pathways.

Discussion

The present studies extend the observations regarding the specialized function of cholangiocytes by identifying and characterizing the elements of the purinergic signaling axis in cholangiocytes derived from distinct functional areas along the intrahepatic bile ducts. Using molecular, pharmacological, and functional biophysical approaches the principal findings in these studies of mouse cholangiocytes are: (1) both small and large cholangiocytes express a repertoire of both P2X and P2Y receptors; (2) both small and large cholangiocytes develop polarized epithelial monolayers with a high transepithelial resistance and demonstrate rapid increases in $[Ca^{2+}]_i$ and transepithelial secretion (I_{sc}) upon exposure to extracellular nucleotides; (3) nucleotide-stimulated secretion is dependent on IP3 receptor-mediated increases in $[Ca^{2+}]_i$ and Ca^{2+}-activated Cl^- channel activation; (4) both small and large cholangiocytes demonstrate mechanosensitive ATP release which is dependent on intact vesicular trafficking pathways; and (5) the magnitude of mechanosensitive ATP release is significantly greater in small versus large cholangiocytes. Thus, these studies demonstrate that both small and large cholangiocytes express all components of the purinergic signaling axis and collectively, provide a working model for mechanosensitive ATP-stimulated secretion along intrahepatic bile ducts. Additionally, the ATP-mediated secretory pathway identified in the mouse small cholangiocytes, which do not exhibit secretin-stimulated secretion,[3,17] represent the first identification of a secretory pathway in these specialized cells. The existence of a gradient along the biliary axis, wherein ATP released from small cholangiocytes "upstream" may represent an important paracrine signal to the "downstream" P2 receptor-expressing large cholangiocytes, has important implications for bile formation (Fig. 8).

Although regulated ATP release has been identified in all liver cells studied, including both human and rat hepatic parenchymal cells and biliary epithelial cells,[20,22] these are the first studies to characterize ATP release in mouse cholangiocytes, and several observations deserve highlighting. First, the magnitude of ATP release from small cholangiocytes was significantly greater than that from large cholangiocytes. Because the mechanism of cholangiocyte ATP release has not been identified, the cellular basis for this difference in

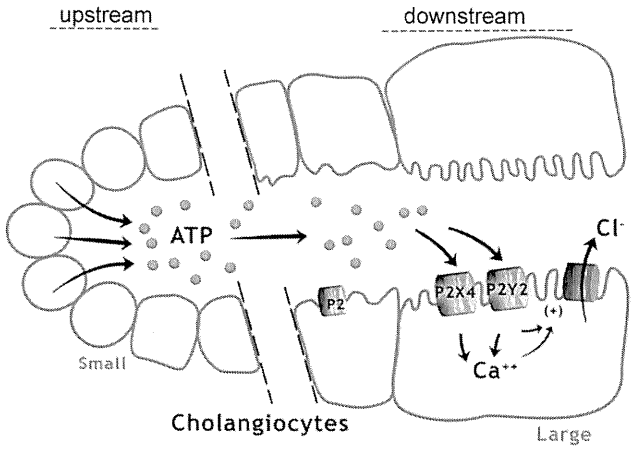

Fig. 8. Proposed model of the purinergic signaling axis along the intrahepatic bile duct. ATP released from small cholangiocytes lining the "upstream" small intrahepatic bile ducts may contribute importantly to local purinergic signaling, serve as a source for ATP in bile, and represent an important paracrine signal to the large cholangiocytes lining the larger "downstream" bile ducts. Both small and large cholangiocytes express a full array of P2 receptors and respond to extracellular nucleotides with increases in $[Ca^{2+}]_i$ and Cl^- secretion.

ATP release cannot be determined. Although CFTR has been proposed as a regulator of ATP release,[12,24,25] MSC do not express CFTR,[17] suggesting alternate ATP release pathways in these cells. One proposed alternate mechanism involves exocytosis of ATP-enriched vesicles. In fact, biliary cells possess a dense population of vesicles ~140 nm in diameter in the subapical space,[26] and increases in cell volume increase the rate of exocytosis to values sufficient to replace ~30% of plasma membrane surface area within minutes. In the current studies, stimuli associated with ATP release were also associated with parallel increases in the rate of exocytosis, and disruption of vesicular trafficking significantly decreased ATP release. Notably, overall rates of exocytosis in response to mechanosensitive stimuli did not vary significantly between MLCs and MSCs, despite a significantly greater release of ATP from MSCs, given the same stimulus. This may suggest the existence of distinct vesicle populations contributing to regulated ATP release. In fact, recent findings in rat liver cells suggest that a distinct population of ATP-enriched vesicles may contribute to regulated ATP release.[27] In some cell types, the concentration of ATP within secretory vesicles may approach 50 mM[28] and, therefore, only several vesicles per cell may account for substantial differences in the concentration of ATP released into the extracellular space. Differences observed in the magnitude of ATP release between MSCs and MLCs may be related to variation in the regulation and/or trafficking of specific vesicles involved in ATP transport (either ATP-containing

vesicles and/or vesicles transporting an ATP transporter to the membrane). This regulation may occur at the level of vesicle "priming", trafficking, or membrane fusion/release, though clearly further work is required. Nonetheless, if these observations apply to *in vivo* conditions, greater ATP release from small cholangiocytes would translate into a significant increase in the concentration of ATP in bile in the "upstream" intrahepatic ducts, given their smaller cross-sectional area and relative volume.[29]

Second, it is notable that extracellular nucleotides elicit secretory responses when applied at both apical and basolateral membranes. The apical membrane specifically represents an anatomic orientation that is well suited for hepatocyte-to-cholangiocyte or cholangiocyte-to-cholangiocyte signaling by release of ATP into bile. This is notably distinct from secretin and other hormones that are delivered to the basolateral membrane through the bloodstream.[1] ATP release from the hepatocyte canalicular membrane may signal to downstream small and large cholangiocytes through apical P2 receptor stimulation in a process known as hepatobiliary coupling. Hepatobiliary coupling has also been described for bile acids, which are released from the hepatocyte canalicular membrane and may be transported into "downstream" cholangiocytes via the apical Na^+-dependent bile acid transporter located on large, but not small, cholangiocytes.[30] Interestingly, Ursodeoxycholic acid is associated with cholangiocyte ATP release and Cl^- secretion.[24] Thus, the ductal concentration of ATP appears to be an important determinant of bile formation and may represent a final common pathway in coupling hepatocyte transport to cholangiocyte secretion.

Lastly, the relative importance of secretin- versus P2 receptor-mediated secretion, in bile formation is unknown. The molecular identity of the Cl^- channel(s) activated in response to ATP remains undefined in biliary epithelium, though it appears to be unrelated to CFTR.[10] Furthermore, although we have previously identified the Ca^{2+}-activated K^+ channels, SK2 and IK-1, in rat and human biliary epithelial cells,[7,8] the expression and contribution of these channels to secretion in mouse cholangiocytes has not been defined.

In conclusion, the present studies represent a functional characterization of the purinergic signaling axis in mouse cholangiocytes from distinct areas of the intrahepatic biliary tree. The findings support a model wherein ATP released from small cholangiocytes lining the "upstream" small intrahepatic bile ducts may contribute importantly to local purinergic signaling, serve as a source for ATP in bile, and represent an important paracrine signal to the large cholangiocytes lining the larger "downstream" bile ducts. Targeting P2 receptor-mediated signaling pathways in intrahepatic biliary epithelial cells may provide new and innovative strategies for stimulating bile formation in the treatment of cholestatic liver diseases.

References

1. Fitz JG. Cellular mechanisms of bile secretion. In: Zakim D, Boyer TD, eds. Hepatology. ed 3. Philadelphia: W.B. Saunders Co.; 1996:362-376.
2. Alpini G, Roberts S, Kuntz SM, Ueno Y, Gubba S, Podila PV, et al. Morphological, molecular, and functional heterogeneity of cholangiocytes from normal rat liver. Gastroenterology 1996;110:1636-1643.
3. Francis H, Glaser S, Demorrow S, Gaudio E, Ueno Y, Venter J, et al. Small mouse cholangiocytes proliferate in response to H1 histamine receptor stimulation by activation of the IP3/CaMK I/CREB pathway. Am J Physiol Cell Physiol 2008;295:C499-C513.
4. Ueno Y, Alpini G, Yahagi K, Kanno N, Moritoki Y, Fukushima K, et al. Evaluation of differential gene expression by microarray analysis in small and large cholangiocytes isolated from normal mice. Liver Int 2003;23:449-459.
5. Martinez-Anso E, Castillo JE, Diez J, Medina JF, Prieto J. Immunohistochemical detection of chloride/bicarbonate anion exchangers in human liver. HEPATOLOGY 1994;19:1400-1406.
6. Chari RS, Schutz SM, Haebig JA, Shimokura GH, Cotton PB, Fitz JG, et al. Adenosine nucleotides in bile. Am J Physiol 1996;270: G246-G252.
7. Feranchak AP, Doctor RB, Troetsch M, Brookman K, Johnson SM, Fitz JG. Calcium-dependent regulation of secretion in biliary epithelial cells: the role of apamin-sensitive SK channels. Gastroenterology 2004; 127:903-913.
8. Dutta AK, Khimji AK, Sathe M, Kresge C, Parameswara V, Esser V, et al. Identification and functional characterization of the intermediate conductance Ca2+-activated K+ channel (IK-1) in biliary epithelium. Am J Physiol Gastrointest Liver Physiol 2009;297:G1009-G1018.
9. McGill J, Basavappa S, Shimokura GH, Middleton JP, Fitz JG. Adenosine triphosphate activates ion permeabilities in biliary epithelial cells. Gastroenterology 1994;107:236-243.
10. Dutta AK, Woo K, Doctor RB, Fitz JG, Feranchak AP. Extracellular nucleotides stimulate Cl- currents in biliary epithelia through receptor-mediated IP3 and Ca2+ release. Am J Physiol Gastrointest Liver Physiol 2008;295:G1004-G1015.
11. Schlenker T, Romac JMJ, Sharara A, Roman RM, Kim S, LaRusso N, et al. Regulation of biliary secretion through apical purinergic receptors in cultured rat cholangiocytes. Am J Physiol 1997;273:G1108-G1117.
12. Minagawa N, Nagata J, Shibao K, Masyuk AI, Gomes DA, Rodrigues MA, et al. Cyclic AMP regulates bicarbonate secretion in cholangiocytes through release of ATP into bile. Gastroenterology 2007;133: 1592-1602.
13. Woo K, Dutta AK, Patel V, Kresge C, Feranchak AP. Fluid flow induces mechanosensitive ATP release, calcium signalling and Cl- transport in biliary epithelial cells through a PKCzeta-dependent pathway. J Physiol 2008;586:2779-2798.
14. Dranoff JA, Masyuk AI, Kruglov EA, LaRusso NF, Nathanson MH. Polarized expression and function of P2Y ATP receptors in rat bile duct epithelia. Am J Physiol Gastrointest Liver Physiol 2001;281: G1059-G1067.
15. Doctor RB, Matzakos T, McWilliams R, Johnson S, Feranchak AP, Fitz JG. Purinergic regulation of cholangiocyte secretion: identification of a novel role for P2X receptors. Am J Physiol Gastrointest Liver Physiol 2005;288:G779-G786.
16. Ishii M, Vroman B, LaRusso N. Isolation and morphologic characterization of bile duct epithelial cells from normal rat liver. Gastroenterology 1989;97:1236-1247.